ATG-101, a tetravalent PD-L1×4-1BB bispecific antibody, augments anti-tumor immunity through PD-L1 blockade and PD-L1-directed 4-1BB activation

Hui Yuwen
Shanghai Antengene Corporation Limited;
Huajing Wang
Oricell Therapeutics Co., Ltd
Tengteng Li
Shanghai Antengene Corporation Limited;
Yijing Ren
Shanghai Antengene Corporation Limited;
Peng Chen
Shanghai Antengene Corporation Limited;
Bohua Li
The Second Military Medical University
David Flowers
Applied BioMath LLC https://orcid.org/0000-0002-7382-8461
Marc Presler
Applied BioMath LLC
Kalyanasundaram Subramanian
Applied BioMath LLC https://orcid.org/0000-0001-9676-5427
Kevin Lynch
Antengene Pty Ltd;
Jay Mei
Antengene Corporation Co., Ltd;
Xiaowen He (peterhe@oricell.com)
Oricell Therapeutics Co., Ltd
Bo Shan (Bo.shan@antengene.com)
Antengene Corporation Co., Ltd
Bing Hou (bing.hou@antengene.com)
Antengene Corporation Co., Ltd https://orcid.org/0000-0002-8348-3831

Article

Keywords:

Posted Date: October 17th, 2022

DOI: https://doi.org/10.21203/rs.3.rs-2146670/v1

Abstract

Immune checkpoint inhibitors (ICIs) have transformed the landscape of cancer treatment. However, only a minority of patients achieve a profound and long-lasting response, and many patients are innately resistant or acquire resistance to ICI therapy. In addition, hepatotoxicity and suboptimal efficacy have hampered the clinical development of agonistic antibodies targeting 4-1BB, a promising immune stimulating target. To effectively target 4-1BB and treat diseases resistant to ICIs, we engineered a tetravalent "2 + 2" PD-L1×4-1BB bispecific antibody (BsAb), ATG-101. ATG-101 binds to PD-L1 and 4-1BB concurrently, with a greater affinity for PD-L1, and potently activates 4-1BB positive T cells when crosslinked with PD-L1 positive cells. ATG-101 also activates exhausted T cells upon PD-L1 crosslinking, indicating a possible role in reversing T-cell dysfunction and exhaustion. ATG-101 revealed potent antitumor activity in numerous *in vivo* tumor models, including those resistant to ICIs or that have progressed following ICI treatment. ATG-101 greatly increased the proliferation of $CD8^+$ T cells, the infiltration of effector memory T cells, and the ratio of $CD8^+$ T/Treg cells in the tumor microenvironment (TME), rendering an immunologically "cold" tumor "hot". ATG-101 is well-tolerated and does not induce hepatotoxicity in non-human primates, even at high doses. According to a computational semi-mechanistic pharmacology model simulation, 4-1BB/ATG-101/PD-L1 trimer formation and PD-L1 receptor occupancy are both maximized at around 2 mg/kg of ATG-101, providing guidance regarding a clinically optimal biological dose. In summary, by localizing to PD-L1-rich TME and activating 4-1BB-positive immune cells in a PD-L1 crosslinking-dependent manner, ATG-101 safely inhibits tumor growth in ICI resistant or refractory animal models.

Introduction

Programmed death-ligand 1 (PD-L1) and programmed cell death protein 1 (PD-1) blockade therapy, or immune checkpoint inhibitors (ICIs), have revolutionized the treatment landscape of multiple malignancies. However, only a minority of patients demonstrate deep and durable responses, with many patients showing innate resistance or subsequently developing resistance to ICI therapy. Tumors with little anti-tumor immune cell infiltration or lack of pre-existing antitumor immune responses are defined as immunologically “cold”. Patients with these tumors have a poor prognosis following PD-(L)1 blocking therapy [1]. On the other hand, malignancies that initially respond well to ICIs may develop acquired drug resistance, frequently as a consequence of T cell exhaustion [2, 3, 4].

4-1BB (CD137, TNFRSF9) is a costimulatory receptor of the tumor necrosis factor receptor superfamily (TNFRSF) and accumulates on the T cell surface upon activation. Receptor stimulation by endogenous 4-1BB ligand (4-1BBL) or agonistic 4-1BB antibodies can markedly augment T cell activation and upregulate inflammatory cytokine response, and lead to the protection against T cell death by upregulation of anti-apoptotic molecules of the B-cell lymphoma 2 (BCL 2) family [5]. 4-1BB expression represents a distinct activation status of highly exhausted $CD8^+$ T cells in tumors [6, 7]. 4-1BB agonism

averts tumor infiltrating lymphocyte (TIL) exhaustion and enhances anti-tumor activity of ICIs [6, 8], providing a rationale for the exploration of 4-1BB targeting immunotherapies in ICI-resistant patients.

Agonistic 4-1BB antibodies have exhibited potent anticancer efficacy in a variety of syngeneic mouse models [9]. However, the on-target-off-tumor liver toxicity has hampered the successful clinical development of therapeutic 4-1BB agonists, such as urelumab, a fully human IgG4 monoclonal antibody [10]. Despite encouraging hints of efficacy, urelumab induced transaminitis at doses ≥ 0.3 mg/kg resulting in a low maximum tolerable dose (MTD, 0.1 mg/kg every 3 weeks) and a suboptimal therapeutic window [9]. The activation of 4-1BB positive liver-infiltrating T cells by the agonistic antibodies has been implicated as the underlying mechanism of liver toxicity [5]. Unlike urelumab, utomilumab, a humanized IgG2 monoclonal antibody, requires Fc-mediated crosslinking to activate the 4-1BB signaling pathway [11, 12]. Utomilumab was better tolerated in patients with a MTD > 10 mg/kg, albeit with a relatively modest anti-tumor activity [13]. The synergy between utomilumab and PD-(L)1 blockade is not significant [14].

One of the most promising next-generation 4-1BB targeting strategies is the use of bispecific antibodies (bsAb) or bispecific fusion proteins, which are designed to be enriched in the tumor microenvironment (TME) enabling tumor cell-mediated 4-1BB activation, thereby minimising on-target-off-tumor toxicity. Typically, such bispecific proteins are composed of a tumor-associated antigen (TAA)-recognizing arm and a 4-1BB-agonistic arm. Several TAA/4-1BB targeting bifunctional proteins, such as HER2×4-1BB [15], CD30×4-1BB [16], B7H3×4-1BB [17], and 5T4×4-1BB [18, 19], have been evaluated in preclinical models, showing potent anti-tumor efficacy with reduced liver toxicity.

The overexpression of PD-L1 in the TME in response to interferon-gamma (IFN-γ) produced by TILs is a critical immune evasion mechanism in a large proportion of cancer patients [20, 21]. The combination of PD-L1 blockade with 4-1BB agonism has shown enhanced anti-tumor responses in preclinical cancer models [6, 8, 22]. Therefore, dual targeting of both PD-L1 and 4-1BB by a bispecific antibody might not only permit tumor cell-mediated 4-1BB activation but may also enable the optimal engagement of anti-tumor immunity.

In this study, we developed a “2 + 2” tetravalent PD-L1×4-1BB BsAb, ATG-101, by introducing lower affinity 4-1BB single chain variable fragments (scFv) into a human IgG1 PD-L1 monoclonal antibody. The mutation on the CH2 domain of the fragment crystallizable (Fc) region abolishes the binding capacity to most FcγRs but preserves the ability to bind to FcRn. ATG-101 binds to PD-L1 and 4-1BB simultaneously, with a greater affinity for PD-L1, and potently activates 4-1BB positive T cells when crosslinked with PD-L1 positive cells. ATG-101 also stimulates PD-1^{+}Tim-3^{+} exhausted T cells in vitro upon crosslinking, indicating a possible role in reversing T-cell dysfunction and exhaustion. ATG-101 demonstrated strong anti-tumor efficacy in a variety of tumor models, including those that were resistant to or had progressed on anti-PD-(L)1 therapy, rendering a "cold" tumor "hot”. ATG-101 was also well tolerated with no evidence of hepatotoxicity in non-human primates (NHPs).

Results

ATG-101 binds to PD-L1 and 4-1BB simultaneously, and blocks PD-1/PD-L1 interaction

ATG-101 is a fully human IgG1-like PD-L1×4-1BB bispecific antibody capable of concurrently binding to human PD-L1 and 4-1BB (hPD-L1 and h4-1BB). The parental antibody sequences of PD-L1 and 4-1BB binding arms were discovered from a phage display human antibody library, followed by 'back to germline' approach and affinity maturation. ATG-101 has a theoretical molecular weight of 196.45kDa. The ATG-101 molecule is structurally comprised of two identical IgG1 heavy chains, two identical light chains, with a short peptide (linker 1) linking a scFv to the C terminal of each heavy chain. The scFv consists of a heavy chain variable domain (VH) and a light chain variable domain (VL) joined by a linker (linker 2) (Fig. 1a).

The fragment antigen-binding (Fab) arm of ATG-101 binds to PD-L1 whilst the scFv recognizes 4-1BB. The binding properties of ATG-101 were evaluated using ForteBio's Octet RED platform. The results demonstrated that ATG-101 could concurrently bind to human PD-L1 and human 4-1BB to create a trimer at the protein level (Fig. 1b). The binding affinity of ATG-101 to hPD-L1-His and h4-1BB-His protein was assessed by surface plasmon resonance (SPR). The binding affinity [dissociation constant (K_d)] of ATG-101 with human PD-L1 (hPD-L1-His) and human 4-1BB (h4-1BB-His) were 0.177 nM and 11.4 nM, respectively (Fig. 1c), reflecting a 64-fold difference in binding affinity. ATG-101 cross-reacted with cynomolgus monkey PD-L1 (K_d=0.043 nM), mouse PD-L1(K_d=1.58 nM) and cynomolgus monkey 4-1BB (K_d=3.57 nM) (Supplementary Fig. 1a). ATG-101 did not compete with utomilumab and only partially competed with urelumab for binding to human 4-1BB, showing that they bind to distinct epitopes (Supplementary Fig. 1b). The > 50-fold higher binding affinity for PD-L1 over 4-1BB of ATG-101 is thought to contribute to the preferential antibody distribution to the TME), with the goal to enhance the therapeutic effectiveness and reduce the likelihood of off-tumor toxicity.

The binding capacity of ATG-101 to cell surface PD-L1 and 4-1BB were determined using flow cytometry. ATG-101 binds to hPD-L1-overexpressed HEK293T cells with a half-maximum effective concentration (EC_{50}) of 2.94 nM. It also binds with an EC_{50} of 8.75 nM to HEK293T cells overexpressing human 4-1BB (Fig. 1d).

In the TME, PD-1 and its ligand PD-L1 perform a vital role in tumor progression and survival by allowing the escape from tumor neutralizing immune surveillance [23]. To evaluate the ability of ATG-101 to block the PD-1/PD-L1 interaction, HEK293T cells overexpressing human or mouse PD-L1 were incubated with serial dilutions of ATG-101. ATG-101 blocked PD-1 protein binding to cell surface expressed PD-L1, with half maximum inhibitory concentration (IC_{50}) of 2.21 and 4.52 nM for human and mouse PD-1/PD-L1 interactions, respectively (Fig. 1e).

To minimize undesired 4-1BB activation through Fc/FcγR-interaction-mediated crosslinking of ATG-101 and FcγR-positive immune cells, the Asparagine 297 on CH2 domain of the Fc region of ATG-101 was mutated to Alanine to eliminate its binding to the majority of FcRs. ATG-101 exhibited weak binding to FcRI, IIa/b, and IIIa, however it maintained binding to FcRn with a Kd of 18.3 nM(Fig. 1f). The binding capacity of ATG-101 to FcRn may prevent the degradation of IgG, and extend its half-life in circulation [24].

ATG-101 potently activates 4-1BB signaling in immunocytes upon PD-L1-crosslinking

One of the primary causes of liver damage generated by 4-1BB agonists is the stimulation of 4-1BB-positive liver-infiltrating T cells [5]. PD-L1-crosslinking-dependent activation of 4-1BB may localize the T cell activation in the TME and reduce off-tumor toxicity. Multiple assays were conducted to establish the agonistic characteristics of ATG-101 towards 4-1BB. ATG-101 activated HEK293T cells expressing h4-1BB that were integrated with nuclear factor κB (NF-κB) fluorescence reporter (293T-h41BB-NF-κB-Luc) in the presence of CHO cells overexpressing human (CHO-hPDL1) or mouse PD-L1 (CHO-mPDL1), with EC50 of 0.39nM and 1.06nM, respectively, while the addition of mock transfected CHO cells did not induce activation of the 4-1BB signaling pathway (Fig. 2a). Furthermore, as a tetravalent “2 + 2” bsAb, ATG-101 induced significantly higher 4-1BB activation compared with a bivalent PD-L1×4-1BB bsAb which incorporates Fabs from parental mAbs of ATG-101 [ATG-101(1 + 1)], suggesting a superior activity of ATG-101 over bivalent PD-L1×4-1BB bsAb (Fig. 2b). In the murine colon carcinoma cell line MC38, elevated cell surface localization of PD-L1 was observed upon stimulation with mouse interferon gamma (mIFN-γ) (Supplementary Fig. 2a). ATG-101 activated 4-1BB signaling in the presence of mIFN-γ-stimulated MC38 cells. However, neither the combined treatment of parental anti-4-1BB and anti-PD-L1 mAbs nor ATG-101 with non-stimulated MC38 induced significant activation of the 4-1BB signaling (Supplementary Fig. 2b, c).

To evaluate the *in vitro* co-stimulatory activity of ATG-101 on primary human T cells, $CD8^+$ T cells were pre-stimulated with anti-CD3 and co-cultured with cell lines expressing different levels of PD-L1. ATG-101 activated $CD8^+$ T lymphocytes to produce interleukin 2 (IL-2) at concentrations of 0.1nM and 1nM, with the quantity of IL-2 production positively correlating with the cell surface expression or total antibody binding sites of PD-L1 (Fig. 2c). In addition, when HEK293 cells expressing PD-L1 (HEK293-PDL1) were co-cultured with parental HEK293 cells in various proportions, ATG-101-induced IFN-γ release increased with the proportion of PD-L1 positive cells. ATG-101 did not activate $CD8^+$ T cells in the absence of PD-L1 crosslinking (HEK293-PDL1 0%) (Fig. 2d). The agonistic activity of ATG-101 was also detected with human peripheral blood mononuclear cells (hPBMCs) stimulated by the superantigen *Staphylococcus aureus* enterotoxin A (SEA). ATG-101 significantly boosted IL-2 production by stimulated-hPMBCs in the presence of CHO-PDL1 cells. In the absence of CHO-PDL1 cells or ATG-101, little IL-2 production was observed (Supplementary Fig. 2d).

Exhaustion of T cells has been linked to the acquired resistance of ICIs [2, 3, 4]. It has been shown that 4-1BB agonism can alleviate T cell exhaustion and that co-stimulation restores the functioning of

exhausted $CD8^+$ TIL *in vivo* [25]. To assess the efficacy of ATG-101 on exhausted T cells, human T cells were isolated, and the cell exhaustion was induced through consistent, strong activation with anti-CD3/CD28 beads for up to 6 days. Upon stimulation with anti-CD3/CD28, the expression of the exhaustion markers PD-1 and Tim-3 were increased (Fig. 2e, f). In the presence of PD-L1 positive cells, ATG-101 enhanced the IL-2 and INF-γ production by the terminally exhausted T cells ($PD\text{-}1^+Tim\text{-}3^+$) and progenitor exhausted T cells ($PD\text{-}1^+Tim\text{-}3^-$) (Fig. 2g), indicating a potential for reversing T cell exhaustion.

Taken together, ATG-101 strongly activates 4-1BB in immunocytes in a PD-L1-crosslinking dependent manner. Agonistic potency correlates positively with PD-L1 expression and the proportion of PD-L1-positive cells.

ATG-101 shows a low risk of inducing cytokine release syndrome (CRS)

Cytokine release syndrome (CRS) is a common adverse event induced by therapeutic immune agonists [26]. The effects of ATG-101 on cytokine release were evaluated utilizing hPBMCs from six distinct donors in both soluble and plate-bound forms of the antibody. The strength of cytokine release induced by ATG-101 at concentrations of 0.3 or 300 μg/mL was significantly less than the positive controls, and no significantly increased cytokine levels were detected in both soluble and plate-bound formats of the cytokine release assays, indicating a low risk of ATG-101-induced CRS at the proposed doses in the clinic (Fig. 2g).

Human umbilical vein endothelial cells (HUVECs) express moderate levels of PD-L1 (Supplementary Fig. 2e). In response to ATG-101, hPBMCs co-cultured with HUVECs released negligible proinflammatory cytokines (Supplementary Fig. 2f). In contrast, in the presence of CHO-hPDL1, which expresses PD-L1 at a much higher level than HUVECs, ATG-101 caused significantly higher levels of cytokine production (Supplementary

Figure 2e, f). These results suggest that ATG-101 poses a low risk of developing CRS in the presence of physiological levels of PD-L1 expression. In addition, an evaluation of *in vivo* cytokine release was conducted as part of a four-week repeated-dose toxicity study followed by a four-week recovery phase. All male and female cynomolgus monkeys treated with 10 mg/kg, 50 mg/kg, and 100 mg/kg ATG-101 had no significant changes in plasma cytokine levels (data not shown).

ES101 (INBRX-105) is a clinical stage “2 + 2” PD-L1×4-1BB bispecific antibody. We compared the ability of ATG-101 and ES101 in stimulating cytokine release in the absence of allogeneic PD-L1 positive cells. PepTivator CMV pp65 is peptide pool consisting of peptides covering the whole sequence of the human cytomegalovirus pp65 protein. Isolated primary $CD14^+$ human monocytes were differentiated into immature dendritic cells (iDCs). Co-culturing iDCs loaded with pp65 peptides with T cells from the same donor served as a primary activation signal for antigen-specific T cells. ES101 induced much greater IL-2 release in the co-culture system than ATG-101 (Supplementary Fig. 2g). This suggests that ATG-101 has a lower risk of inducing CRS or other off-tumor toxicity compared with ES101.

ATG-101 shows potent anti-tumor effect in vivo

The *in vivo* anti-tumor efficacy of ATG-101 was evaluated in h4-1BB humanized mice (C57BL/6) bearing murine MC38 colon tumors, B16F10 melanoma, or Pan02 pancreatic tumors (Fig. 3; Supplementary Fig. 3).

The *in vivo* efficacy of ATG-101 in the MC38 model was previously described in our patent, where mice with an average tumor volume (TV) of 60 mm^3 were administered with phosphate buffered saline (PBS) control, ATG-101, parental 4-1BB mAbs, parental PD-L1 mAbs, or a combination of 4-1BB and PD-L1 parental mAbs twice weekly. ATG-101 at 7.5 mg/kg exhibited a higher tumor growth inhibition rate compared to anti-4-1BB mAb or anti-PD-L1 mAb, with a tumor growth inhibition (TGI) of 109% on Day 15 after treatment commencement. The efficacy of the combination of 4-1BB and PD-L1 mAbs was comparable to that of ATG-101[27].

To further evaluate the anti-tumor efficacy of ATG-101 on large, established tumors, IgG-Fc (10 mg/kg, control), and ATG-101 at 3.25 and 13 mg/kg (once every 3 days for a total of 6 doses, Q3D×6) were delivered to mice carrying MC38 tumor with an average TV of 239 mm^3. Compared to the IgG-Fc control, ATG-101 treatment significantly suppressed tumor growth and prolonged the survival of tumor-bearing mice, without reducing body weight (Fig. 3, a-c; Supplementary Fig. 3a). The average TGI on Day 20 of 3.25 and 13 mg/kg ATG-101 doses were 93.0%, and 97.7%, respectively. Particularly, on Day 69, two out of six mice treated with 13 mg/kg ATG-101 rejected the tumor completely (Supplementary Fig. 3a). The two tumor-free animals were re-challenged with the MC38 cells, and these mice did not acquire tumors, indicating the establishment of immunological memory in response to ATG-101 (Fig. 3d).

In addition, the efficacy of ATG-101 was investigated in h4-1BB humanized mice bearing B16F10 syngeneic melanoma tumors, a model considered to be an immunologically ‘cold’ tumor. Mice were administered with PBS, IgG, ATG-101, utomilumab, atezolizumab or the combination (utomilumab and atezolizumab), respectively (Q3D×5). ATG-101 was well tolerated, with no substantial weight loss or serious side effects (Supplementary Fig. 3b). ATG-101 at 3.25 and 13 mg/kg exhibited greater tumor growth inhibition compared with utomilumab, atezolizumab or the combination, with TGI of 55.74%, 57.42%, 26.03%, 30.52%, and 40.75%, respectively, on Day 10 (Fig. 3e, and Supplementary Fig. 3c). In addition, ATG-101 at a dose of 13 mg/kg demonstrated a significant survival advantage over the control groups (Supplementary Fig. 3d).

Finally, in h4-1BB humanized mice (C57BL/6J) bearing Pan02 murine pancreatic tumors, atezolizumab did not show anti-tumor efficacy at 7.5mg/kg, while ATG-101 at a molar equivalent dosage of 10 mg/kg was well tolerated and significantly inhibited tumor growth, resulting in 78.48% TGI on day 24 (Fig. 3f, g; Supplementary Fig. 3e). This data suggests that ATG-101 has the potential to treat cancers with primary resistance to anti-PD-(L)1 therapies.

Taken together, ATG-101 demonstrated potent *in vivo* anti-tumor activity in mouse tumor models, including those with large established tumors, immunologically “cold” tumors, and tumors with primary

resistance to ICIs.

ATG-101 bolsters anti-tumor immunity in the tumor microenvironment

To determine the pharmacodynamic (PD) effects of ATG-101, h4-1BB humanized mice bearing MC38 tumors were treated with IgG control or ATG-101 (9.9 mg/kg) on Day 0 and Day4 after grouping. Treatment with ATG-101 resulted in tumor growth inhibition (Fig. 4a). 48 hours after the last dose administration, T cells were isolated from tumor, liver, spleen and blood, and analyzed by flow cytometry (Fig. 4b). ATG-101 dramatically increased the infiltration of cytotoxic $CD8^+$ T cells and the ratio of $CD8^+$ T cells/regulatory T cells (Treg) in the tumor, compared to the control group. Interestingly, increased Treg levels and a decreased $CD8^+$ T/Treg ratio were detected in blood and liver in response to ATG-101, possibly due to a compensatory effect (Fig. 4b). The decreased $CD8^+$ T/Treg ratio in liver suggested an anti-inflammatory state and decreased risk of ATG-101-induced liver damage.

To further evaluate the impact of ATG-101 on tumor infiltrating immune cells, h4-1BB humanized mice bearing lymphoma EL-4 tumors were dosed with PBS or IgG (10 mg/kg), or 3.25 and 13 mg/kg ATG-101, once every 3 days (Q3D) for a total of 4 doses. ATG-101 at 3.25 and 13 mg/kg exhibited significant tumor growth inhibition compared to PBS or IgG group, with TGIs of 35% and 50%, respectively (Fig. 4c). Compared to PBS and IgG controls, ATG-101 at 3.25 and 13 mg/kg significantly boosted the proliferation of $CD8^+$ T cells, infiltration of effector memory T cells, and $CD8^+$ T/Treg ratio in the TME. Specifically, 13 mg/kg ATG-101 increased the infiltration of late activated T cells and Natural killer T cells (NKT) by 5 and 2.5 folds, respectively. These findings suggest that ATG-101 may enhance anti-tumor immunity in the TME.

ATG-101 demonstrates in vivo **efficacy in a tumor model progressing on anti-PD-L1 treatment**

Malignancies that initially respond to ICIs may subsequently develop acquired drug resistance [3]. To evaluate the potential of ATG-101 in treating diseases with acquired resistance to ICI, anti-tumor activity of ATG-101 in a MC38 tumor model progressing on anti-PD-L1 treatment was tested. Mice bearing MC38 tumors were treated with anti-PD-L1 initially to achieve tumor growth inhibition and upon disease progression, half of the mice were switched to ATG-101 ("atezolizumab to ATG-101"), while the other half remained on anti-PD-L1 treatment (atezolizumab) (Fig. 5a - c). Progression of disease (PD) was defined when all the following conditions were met: during three consecutive measurements of tumor volume from an individual mouse, i) TV > 200 mm^3 at the first measurement; ii) the tumor size keeps growing and the growth rate accelerates between measurements; and iii) the increase% in tumor size (ΔTV) > 25% between two measurements (Supplementary Fig. 4a). Both atezolizumab and “atezolizumab to ATG-101” inhibited tumor growth compared to the control group, whereas ATG-101 induced growth inhibition or regression in tumors that had progressed on atezolizumab (Fig. 5, a, b). Additionally, "atezolizumab to ATG-101" resulted in a significant survival advantage over atezolizumab or the control group (Fig. 5c). Furthermore, tumor specimens were collected at the end of the study, and the cell types in the TME were

analyzed using multiplex immunofluorescence staining. ATG-101 significantly increased the number of $CD8^+$ T cells (effector T cells) and $CD4^+$ T cells (helper T cells) in the TME, compared to the control or atezolizumab groups (Fig. 5d, e; Supplementary Fig. 4b).

ATG-101 is well tolerated in a 4-week GLP repeated dose toxicity study with no observed liver toxicity in cynomolgus monkeys

The potential toxicity profile of ATG-101 was examined in a GLP-compliant 4-week repeated dose toxicity study in cynomolgus monkeys via IV infusion, followed by a 4-week recovery period. Five male and female animals per group were administered with 0 (0.9% sodium chloride injection), 10, 50, or 100 mg/kg of ATG-101 weekly. Three male and female animals per group were necropsied at the completion of the dosing period, and the remaining two animals were allowed to recover for 28 days. During the study, there were no significant changes in serum alanine transaminase (ALT) and aspartate transaminase (AST) concentrations between ATG-101 groups and vehicle groups at any time point, indicating that ATG-101 exhibited no hepatotoxicity in cynomolgus monkeys even at the 100 mg/kg dose level. (Fig. 6a, b). No ATG-101-related macroscopic findings in liver were observed in all treatment groups (Fig. 6c). The highest non-severely toxic dose (HNSTD) of ATG-101 was determined to be 100 mg/kg.

A receptor occupancy (RO) study was also performed to measure the changing conditions of PD-L1 RO rate on $CD3^+$ T cells during the GLP toxicology study. On D1, 2 hours following the initial dose, the RO of each ATG-101-dosing group was close to 100% (97.04%-103.86%). Throughout the dosing and recovery period (D14, D28, D43, and D57), the receptor occupancy at 10, 50, and 100 mg/kg maintained at or above 83.28% (83.28%-110.13%), indicating adequate exposure to the ATG-101-related targets during the experiment (Fig. 6d). In addition, the long-term persistence of high ATG-101 RO shows the possibility of a prolonged clinical effect.

A computational semi mechanistic pharmacology model of ATG-101 provides a rational basis for clinical dose selection and prediction of optimal biological dose

A quantitative systems pharmacology (QSP) model for ATG-101 was developed to predict clinical starting and efficacious doses for first-in-human studies using the available preclinical data (Fig. 7a). The 3-compartment model predicts the formation of the tetrameric complex between the ATG-101, 4-1BB, and PD-L1, referred to as the “trimer,” as well as the receptor occupancy to individual targets. This allows the model to quantify 4-1BB-driven activation as well as checkpoint blockade along the PD-1: PD-L1 axis. The binding parameters (e.g., individual target affinities, the avid trans-cell complex formation rates) were calibrated to *in vitro* pharmacodynamic readouts (on-cell binding, NF-kB signaling, etc.) and validated against PD1-blocking assays and IL-2 release (Fig. 7b).

Human predictions were performed by translating the calibrated binding parameters with human-specific parameters for receptor concentrations, receptor turnover, drug transport, and elimination (See Materials and Methods). Predicted time series for the PK in blood as well as trimer formation and PD-L1 receptor occupancy in the tumor compartment are shown in Fig. 7c for Q3W dosing. Given the uncertainty in the

avidity parameters of the trans-cell binding and the clinical variability of PD-L1 expression, high and low bookend values were carried forward in the analyses. To assess a starting dose based on Minimal Anticipated Biological Effect Level (MABEL), 20% of maximum trimer formation in the tumor compartment was chosen as a metric (these trimer levels correspond to increases in 4-1BB signaling above background *in vitro*).

The model was then used to evaluate an appropriate efficacious dose that gives the overall best efficacy on both the 41BB-activation and checkpoint inhibition axes. Note that at high doses, the formation of trimer is inhibited because the potential cross-arm binding receptors are occupied by single-bound drug molecules, a phenomenon common to all bispecific molecules[28]. This presents a potential tradeoff between complete coverage of PD-L1 with the optimal formation of trans-cell complexes (Fig. 7d). The most favorable regimen lay at a high PD-L1 RO with maximal trimer formation at a single dose level. The ability to achieve this balance depends on the overall avidity of the molecule, especially the trans-cell binding. The model-predicted landscape of trimer vs PD-L1 RO for ATG-101 is visualized in Fig. 7e. Even in a range of parameter regimes given the uncertainty in the model, trimer and PD-L1 RO are both maximized at approximately 2 mg/kg (Fig. 7e, f).

For context, a comparator molecule GEN1046 (Genmab) was calibrated with a similar method using publicly available data. GEN1046 also binds to 4-1BB and PD-L1, but with a 1:1 structure rather than the 2:2 valency of ATG-101. The two molecules were compared in a head-to-head simulation. ATG-101 dosed at 2 mg/kg (140 mg) Q3W is predicted to achieve greater than 90% trimer formation and greater than 90% PD-L1 RO. At 0.3 mg/kg (21 mg) Q3W, GEN1046 is predicted to achieve maximum tumor trimer formation but only occupies about 55% of PD-L1 in the tumor compartment. At 0.6 mg/kg (42 mg) Q3W, GEN1046 is predicted to occupy 90% of tumor PD-L1 but will only form about 65% of its maximal trimer levels (Fig. 7f).

To validate these results, *in vitro* 4-1BB activation experiments were performed with the full version of ATG-101 and a monovalent format similar to the GEN1046 structure (Fig. 7g). The binding results indicate a similar trend as predicted by the systems pharmacology model. This demonstrates the differences in format can affect the overall avidity of the molecule in ways that are consistent with the model predictions between the two molecules.

Overall, these simulations predict that ATG-101 is less susceptible than GEN1046 to loss of trimer formation at higher doses due to its stronger cross-target binding. This may allow the drug to be dosed such that the benefits of 41BB activation and checkpoint inhibition are maximized simultaneously, while presenting a safe therapeutic for patients (Fig. 7h).

Discussion

The clinical development of agonistic 4-1BB antibodies has been hampered by hepatotoxicity (urelumab) or suboptimal efficacy (utomilumab) [5]. Bifunctional proteins targeting both a TAA and 4-1BB have been

investigated in clinical trials and preclinical models, and they have been shown to circumvent these difficulties by inducing tumor cell-mediated 4-1BB agonism [15, 16, 17, 29]. PD-L1 is frequently over-expressed in the TME, and its inhibition exhibits synergy with 4-1BB agonists [6, 8, 22]. As a tetravalent PD-L1×4-1BB BsAb, ATG-101 potently activates 4-1BB positive T cells in a PD-L1-crosslinking dependent manner. The higher affinity of PD-L1 binding versus 4-1BB binding ensures TME-distribution of ATG-101, and the deficiency of FcγRs binding ensures that ATG-101 shows 4-1BB agonist activity only when crosslinked by PD-L1 positive cells. As a result, ATG-101 strongly inhibits the growth of anti-PD-(L)1 resistant tumors *in vivo*, without causing liver damage in cynomolgus monkeys at doses levels up to 100 mg/kg.

Optimal biological dose (OBD) is generally defined as the lowest tolerable dose providing the highest rate of efficacy in patients [30]. The “sweet spot” we defined here is the dose that provides the drug’s saturated biological activity while being able to be safely administered. The biological activity of a PD-L1x4-1BB bispecific is primarily mediated by two mechanisms: i) PD-L1 crosslinking-dependent 4-1BB activation, which occurs as a result of PD-L1-antibody-4-1BB trimer formation; and ii) blockade of PD-1/PD-L1 interaction, the rate of which can be estimated by the RO of PD-L1. Therefore, the saturation biological activity is supplied by maximal trimer formation in addition to 100% PD-L1 RO. GEN1046, a "1 + 1" bivalent bsAb, is the most advanced PD-L1×4-1BB bispecific antibody. It has demonstrated encouraging early clinical activity in a heavily pretreated patient population with advanced solid tumors, including those resistant to prior anti-PD-(L)1 treatments [31, 32]. In addition, GEN1046 appears to have a manageable safety profile with flat dosages up to 1200 mg [32]. However, a much lower 100 mg flat dose of GEN1046, which was predicted to yield only 70% PD-L1 RO [33], was chosen for the dose expansion phase and the combination with anti-PD-1 is being evaluated in a clinical trial [34]. This was owing to the fact that greater dosages resulted in decreased trimer formation or the "hook effect" [33]. These findings suggest that although being safely administered, GEN1046 could not reach a dose level at which it could deliver saturated biological activity.

The formation of this trimeric complex is subject to various factors such as binding affinity to each target, avidity effects between the two targets, the density of target receptors, and the effector–target (E:T) ratios. While these trimeric complexes are difficult to detect directly, they can be predicted via mechanistic modeling. By our QSP modeling, ATG-101 dosed at 2 mg/kg (140 mg) Q3W is projected to achieve greater than 90% trimer formation and greater than 90% PD-L1 RO in humans, suggesting the potential of ATG-101 to hit the “sweet spot” in clinic. Meanwhile, consistent with the clinical observation of GEN1046’s “hook effect”, modeling results indicate that at 0.3 mg/kg (21 mg) Q3W, GEN1046 may induce maximal trimer formation but only occupies approximately 55% of tumor PD-L1. At higher doses, GEN1046 can occupy more tumor PD-L1 but forms fewer trimers. Additionally, the simulation implies that tetravalent binding of the "2 + 2" bispecific antibody may result in greater trimer formation and reduced hook effect than the "1 + 1" format, as demonstrated here.

INBRX-105 (ES101) is a clinical stage “2 + 2” PD-L1×4-1BB bispecific antibody. During Phase 1 dose escalation study, dose-limiting liver toxicity was observed at multiple dose levels and the MTD of INBRX-

105 was determined to be 1 mg/kg [35]. However, at MTD, INBRX-105 may not completely occupy PD-L1. The combination of INBRX-105 and pembrolizumab will be explored in a Phase 2 study [36]. Although the binding affinity for 4-1BB was not compared directly between ATG-101 and INBRX-105, INBRX-105 demonstrated a stronger autologous PBMC activation when DCs were loaded with viral antigen, implying a more robust 4-1BB agonistic activity than ATG-101. We believed that by balancing the affinity/avidity of PD-L1 and 4-1BB binding, ATG-101 may be able to avoid the decoupling of 4-1BB activation and PD-L1 RO, as has been observed with GEN1046 due to “hook effect” or INBRX-105 due to 4-1BB activation related liver toxicity and thus achieve a clinically optimal effect.

Anti-PD1/PDL1 therapy has shown great success in the treatment of malignancies. However, only a small subset of patients exhibit deep and durable clinical responses, and many of those who initially respond are likely to develop acquired resistance[37]. Numerous mechanisms have been proposed to account for the primary or acquired resistance of ICIs. MHC dysfunction induced by B2M mutations [38], resistance of IFN-γ signaling caused by JAK1/2 mutation [39], and alternations of some oncogenic genes, such as STK11 and KRAS [40] have been reported to confer resistance to anti-PD1/PDL1 treatment. A “cold” TME is one of the major causes for the primary resistance to ICI treatment [41]. TME is the complex and diverse multicellular environment in which the tumor thrives [42]. Tumors with little anti-tumor immune cell infiltration in the TME or lack of pre-existing antitumor immune responses due to immunosuppressive TME have been defined as “cold”, and have characteristically poor response to ICIs [1, 41]. B16F10 is a “cold”, syngeneic murine melanoma model with poor immune cell infiltration [43]. Monoclonal antibodies targeting PD-L1 or 4-1BB shows little anti-tumor efficacy in the B16F10 model, while ATG-101 demonstrated potent anti-tumor activity. EL-4 is a syngeneic murine T cell lymphoma model which is resistant to anti-PD-L1 treatment [44]. ATG-101 inhibited EL-4 growth in a dose-dependent manner. Notably, ATG-101 significantly increased the infiltration, proliferation and activation of $CD8^+$ T cells, the infiltration of NKT cells, and the $CD8^+$/Treg ratio in the tumor microenvironment, implying a role in turning “cold” tumors “hot” and increasing anti-tumor immunity. This may be the underlying mechanism of ATG-101’s activity in treating ICI resistant tumors.

ICI treatment-induced compensatory inhibitory signaling, such as upregulation of Tim3 [45, 46] or LAG3 [47, 48], and T cell exhaustion are two of the primary causes of acquired ICI resistance [2, 3, 4]. In the presence of PD-L1 positive cells, ATG-101 stimulated the release of IL-2 and IFN-γ by $PD\text{-}1^+Tim3^+$ exhausted T cells. In a MC38 mouse tumor model, ATG-101 produced substantial growth suppression or regression of tumors progressing after anti-PD-L1 treatment. These results suggest the potential of ATG-101 for the treatment of diseases with ICI-acquired resistance via the re-activation of exhausted T cells.

In summary, the preclinical results illustrated in this study are consistent with the contention that ATG-101 will provide safe and effective combined PD-L1 antagonism and tumor-specific 4-1BB agonism. A phase I, multicenter, dose-escalating clinical trial evaluating ATG-101 in patients with solid tumors and hematologic malignancies is ongoing [49].

Methods

Binding capability of ATG-101 to hPD-L1/h4-1BB by ForteBio

ATG-101 was biotin labeled (Thermo, A39257) and purified with desalting column (Thermo, 89890) as manufacturer's instructions. The concentration of biotinylated protein was measured using a BCA kit (Thermo Pierece, 23225). Biotinylated ATG-101 at 100 nM was captured on SA biosensor, followed by loading first protein hPD-L1-Fc (Sino Biology, 10377-H05H) or h4-1BB-Fc (ACROBiosystems, 41B-H5258)) at 100 nM for 5 minutes, then loading the second protein h4-1BB-Fc (or hPD-L1-Fc) at 100 nM for 5 minutes, IgG-Fc was used as control. Firstly, ATG-101 was labeled with biotin and immobilized on the Streptavidin (SA) biosensors. Injection of human 4-1BB-Fc fusion protein resulted in the detection of a binding signal, indicating the formation of ATG-101-4-1BB complexes. The addition of human PD-L1-Fc fusion protein elicited a second signal. Injection of hPD-L1 followed by h4-1BB protein had a comparable effect.

Binding affinity of ATG-101 to hPD-L1/h4-1BB protein by Biacore

Biacore running buffer was 1×HBS-EP + Buffer prepared from 10×HBS-EP + Buffer (GE Healthcare, BR-1006-69). An anti-human IgG chip was prepared by immobilizing antihuman IgG Fc antibody via amine coupling (GE Healthcare, BR-1003-50) on 1–8 flow cells a CM5 chip (GE Healthcare, 29-1496-03). The sensor chip surfaces were then flushed with HBS-EP + buffer to stabilize the baseline. Then 25 nM hPD-L1 (ACROBiosystems, PD1-H5229) solution was 2-fold serially diluted and 50 nM h41-BB (ACROBiosystems, 41B-H5227) solution was 2-fold serially diluted. The serially diluted hPD-L1 and h4-1BB were injected into flow cells 3 and 4 sequentially. The association and dissociation time were 180 and 400 seconds, respectively. The surface was regenerated with 10 mM Glycine pH 1.5 (GE Healthcare, BR-1003-54) by injecting into flow cells 3 and 4 at 30 μL/min for 30 seconds followed by a stabilization period of 60 seconds. Binding kinetics was calculated using Biacore Insight Evaluation Software (Version 2.0.15.12933) and a 1:1 binding model for curve fitting.

Binding affinity of ATG-101 to FcγRs and FcRn by ForteBio

Biotinylated hFcγRIIIA (ACROBiosystems, CD8-H52H4) was loaded to the SA sensor (PALL Life Sciences ForteBio, 18-5019) for 2 minutes. Then 2-fold serially diluted ATG-101 down from 750 nM was loaded to bind for 2 minutes then dissociating for 2 minutes. Ni-NTA sensor (ForteBio18-5101) was used for the other Fc receptors. Loading 15nM FcRs [hFcγRI (ACROBiosystems, FCA-H52H2), hFcγRIIA (ACROBiosystems, CDA-H5221), hFcγRIIB (ACROBiosystems, CDB-H5228), FcRn (ACROBiosystems, FCM-h5286)] for 6 minutes, then loading 2-fold serial diluted ATG-101 from 1000 nM for 3 minutes. The dissociation was performed with Ni-NTA sensor for 10 min. Data was analyzed using Data Analysis 9.0.

Binding affinity of ATG-101 to hPD-L1/h4-1BB by flow cytometry

HEK293T cell overexpressing human PD-L1 (293T-hPDL1) and HEK293T cells overexpressing h4-1BB (293T-h41BB) cells were incubated with serial dilutions of ATG-101 at 4°C for 1 hour respectively, followed by fluorophore (PE) anti-human IgG secondary antibody (Abcam, ab98596) and APC anti-human IgG secondary antibody (Biolegend, 410712) for 30 minutes at 4°C, respectively. Mean fluorescence intensity (MFI) was measured with High-throughput flow cytometry.

Blockade of PD-1/PD-L1 interaction with ATG-101

Biotinylated human or mouse PD-1 at a final concentration of 40 μg/ml and serially diluted ATG-101 or its PD-L1 parental antibody were cocultured with 293T-hPDL1 or 293T-mPDL1 cells. Then incubated for 1 hour at 4°C, followed by Streptavidin and PE (Biolegend, 405204) for 30 minutes at 4°C at 1:500 ratio. The high-throughput flow cytometer was used to determine mean fluorescence intensity (MFI).

PBMC Cytokine Release

The effect of ATG-101 on PBMC cytokine release was detected in both soluble and plate-bound format. For soluble format, serial diluted ATG-101, isotype control and single concentration of OKT3 (Biolegend, 317326) and LPS (Sigma, L4391) were added to 48-well cell culture plates at 40 μL per well, duplicate. OKT3 and LPS were used as positive control. Then, 360 μL fresh PBMC form 6 different donors (Saily) were separately seeded to the plates at 2×10^5 cells per well. For plate-bound format, test articles were coated on 48-well cell culture plates overnight at 4°C at 400 μL per well. Then, the coating solutions were removed and 400 μL fresh PBMC were seeded to the plates at 2×10^5 cells per well. All the plates were incubated at 37°C with 5% CO2 for 48 hours. Supernatants were collected and then analyzed by electrochemiluminescence analyzer (MSD, MESO® Sector S600) using V-PLEX Plus Proinflammatory Panel 1 (human) Kit to detect the cytokines (TNF-α, IL-1β, IL-6) (MSD, K15049G).

In vivo efficacy study on murine syngeneic tumor models

h4-1BB knock in (KI) mice [hCD137 (4-1BB) mice, C57BL/6-Tnfrsf9], whose 4-1BB gene is replaced by the h4-1BB gene, were supplied by Beijing Biocytogen, Inc. or Shanghai Model Organisms Center, Inc. These mice were housed in an SPF barrier. Six to eight-week-old female h4-1BB KI mice were used for animal experiments. For all groups, the route of drug administration was intraperitoneal injection. Body weight was recorded, and the tumors were measured with digital calipers 2–3 times per week. Tumor volumes were calculated by the formula: $\text{length}\times\text{width}^2\times0.5$. The animals were euthanized at the end of the study. Detailed methods for each mice study are as follows.

MC38 colon cancer xenograft model (starting tumor volume = 60 mm^3)

MC38 cells were inoculated subcutaneously into the right side of h4-1BB humanized mice (supplied by Beijing Biocytogen, Inc) at a concentration of 3×10^6 cells/0.2 mL. When the tumor volume reached a size of about 60 mm^3, they were separated into six groups based on tumor volume, 5 mice for PBS group and 6 mice for the other groups. The mice were intraperitoneally injected with PBS (vehicle control), IgG (isotype control, 7.5 mg/kg), atezolizumab (7.5 mg/kg), Avelumab (7.5 mg/kg), parental PD-L1 antibody (7.5 mg/kg), and parental 4-1BB antibody (3 mg/kg), ATG-101 (7.5 mg/kg) and parental PD-L1 antibody (7.5 mg/kg) + parental 4-1BB antibody (3 mg/kg) twice a week for 2 weeks.

MC38 colon cancer xenograft model (starting tumor volume = 239 mm^3)

The MC38 cells were inoculated subcutaneously on the right side of h4-1BB humanized mice (supplied by Beijing Biocytogen, Inc) at a concentration of 5×10^5 cells/0.1mL. When the tumor volume grew to about 239 mm^3, mice were randomly divided into each group, 6 mice per group. The mice were intraperitoneally injected with IgG (10 mg/kg) or ATG-101 (3.25 and 13 mg/kg). 13 mg/kg ATG-101 and 10 mg/kg IgG (or monoclonal antibody) gave a comparable molar concentration. Treatment was provided six times continuously on day 0, 3, 6, 9, 12, and 15, and the efficacy project study terminated on day 69 for all groups. Mice with a completely eradicated tumor in the efficacy study were re-challenge with MC38 on day 42, whereas three control mice were newly injected with the tumor cells at the same time.

B16F10 melanoma xenograft model

The h4-1BB humanized mice (supplied by Shanghai Model Organisms Center, Inc) were implanted with 5×10^5 B16F10 cells. Tumor-bearing mice were randomly divided into seven groups based on tumor volume (average TV $\approx$ 48 mm^3) and then treated with test articles on day 5, 8 mice per group. The mice were intraperitoneally injected with PBS, IgG (10 mg/kg), atezolizumab (10 mg/kg), utomilumab (4 mg/kg), ATG-101 (3.25 and 13 mg/kg), and atezolizumab (10 mg/kg) + utomilumab (4 mg/kg).

Pan02 pancreatic cancer xenograft model

Each female C57BL/6 mouse (supplied by Beijing Biocytogen, Inc) was inoculated subcutaneously in the right front flank region with Pan02 tumor cells ($3x10^6$) in 0.1 ml of PBS for tumor development. The randomization was started when the mean tumor size reached approximately 149 mm^3. 24 tumor bearing mice were enrolled in these groups and randomly assigned to 3 study groups. The inoculation date was defined as day 0. All of mice were injected intraperitoneally, IgG (7.5 mg/kg), Aterzolizumab (7.5 mg/kg) or ATG-101 (10 mg/kg) once every three days.

Drug pharmacodynamic (PD) effect in the MC38-hPD-L1 xenograft model

MC38-hPD-L1 cells were inoculated subcutaneously into the right flank of h-41BB humanized mice (supplied by Beijing Biocytogen, Inc) at a concentration of 5×10^5 cells/0.1mL. When the tumors volume

reached about 281 mm^3, the mice were randomly divided into two groups based on tumor size (4 mice per group). Both groups received intraperitoneal injections with IgG (7.5 mg/kg) or ATG-101 (9.9 mg/kg) on day 0, every two days for two times. The experiment was terminated 48 hours after the last administration, and the animals were euthanized at the conclusion. The body weight and tumor volume of the mice were measured, and the tumor, spleen, and liver were excised and weighed. Blood was collected, digested, and processed into a single cell suspension for flow cytometry analysis. $CD8^+$ T cells and Treg cells ($CD25^+$ & $Foxp3^+$) were analyzed with antibodies against CD45 (Biolegend 103188), CD3 (Biolegend 100210), CD4 (Biolegend, 100438), CD8 (Biolegend 100759), CD25 (Biolegend 102008) and Foxp3 (eBioscience, 25-5773-82).

In vivo efficacy and PD evaluation in EL-4 xenograft model

The mice were subcutaneously inoculated with 5×10^5 EL-4 cells on the right side of h4-1BB humanized mice (supplied by Shanghai Model Organisms Center, Inc). When the average size of the tumor reached 71mm^3, randomization was performed based on the tumor size. The inoculation date was defined as day 0. All of mice were injected intraperitoneally every two days. On Day 10, all groups (8 mice per group) were treated with PBS (vehicle control), IgG (isotype control, 10 mg/kg), and ATG-101 (1, 3.25, 13 mg/kg), and mouse tumors were collected for flow cytometry analysis. All samples were processed into single cell suspensions and stained cells followed by flow cytometry data collecting. Tumor cells were analyzed using viability dye for live/dead cells and fluorochrome conjugated antibodies against human CD45 (BioLegend, 103138) as a leukocyte marker. Expression of T cell and NK cell markers was analyzed using fluorochrome-conjugated antibodies against CD3 (BD Biosciences, 740268), CD8 (BioLegend, 100705) and CD4 (BioLegend, 100438), CD25 (BioLegend, 102012), CD69 (BioLegend, 104536), CD44 (BioLegend, 103032), CD62L (BioLegend, 104440), Foxp3 (eBiosciences, 12-5773-82), Ki67 (eBiosciences, 56-5698-82), and CD335 (BioLegend, 137619). Cell population marker: $CD3^+$ $CD4^+$: CD4 T helper cells; $CD3^+CD8^+$: CD8 T cytotoxic T cells; $CD4^+CD25^+Foxp3^+$: Regulatory T cells; $CD44^+CD62^-$: Effector memory T cells; CD25 and CD69: activation marker; Ki67: proliferation marker; $CD3^+CD335^+$: NKT cells. Data was analysis with Kaluza 2.1 software for various immune cell ratios.

In vivo efficacy of ATG-101 in atezolizumab-progressed MC-38 syngeneic mouse model

The h4-1BB humanized mice (supplied by Beijing Biocytogen, Inc) were inoculated subcutaneously in the right rear flank region with 1 x 10^6 MC38 tumor cells in 0.1 ml of PBS for tumor development. Mice were randomized when the mean tumor size reached approximately 51 mm^3. The date of randomization was designated as day 0, and treatments were commenced began on that day. After randomization, mice were treated with PBS (vehicle control, 6 mice per group) and atezolizumab (10 mg/kg, 14 mice per group). Atezolizumab was dosed to the disease progression group initially (14 mice per group), and when an individual mouse reached the pre-defined onset of disease progression, ATG-101 (13 mg/kg) would be dosed as the replacement medication for the mouse; for progression-free animals, atezolizumab monotherapy would be maintained. At the end of the study, tumors were collected, formalin fixed, and

paraffin embedded (FFPE) blocks were produced, and sections were sectioned with a manual rotary microtome, 4 m thickness/section. CD8 (Cell Signaling, 98941), CD4 (Cell Signaling, 25229), F4/80 (Cell Signaling, 70076), MHCII (Invitrogen, 14-5321-82), FoxP3 (Cell Signaling, 12653), PD-L1 (Abcam, ab174838) and DAPI (Sigma, 28718-90-3) staining were all performed by multiplex immunohistochemistry (IHC). Goat anti Rb IgG (Leica, DS9800 and Vector, MP-7444) were used as secondary antibodies. Vectra Polaris automated image system (Akoyabio) and inForm image analysis software was used to capture the pictures.

Toxicity study of ATG-101 in cynomolgus monkeys with a 4-week recovery period

ATG-101 was given to four groups of cynomolgus monkeys, each with five males and five females, once a week at doses of 0 (0.9 percent sodium chloride injection), 10, 50, and 100 mg/kg. After treatment was ended, 3 animals/sex/group were necropsied at the end of the dosing period, and the surviving animals proceeded to recover for 28 days, and 2 animals/sex/group were necropsied at the end of the recovery period. **ALT/AST test**: Blood was collected before feeding. Samples were collected into the tubes with separation gel and coagulant and centrifuged to obtain serum. The Hitachi-7180 Automatic Clinical Analyzer was used to evaluate serum samples. **Receptor occupancy (RO)**: AF647 labeled ATG-101 parental anti-PD-L1 mAb YN035 (AF647-YN035) was employed to assist in the measurement of free receptor occupancy rate of $CD3^+$ T cells. Each test sample was divided into two wells (well A and well B). The well A was treated with saturating concertation of ATG-101 while the well B was only sample as non-specific fluorescence adsorption control (namely background fluorescence signal). The fluorescence signal of test sample was the recorded fluorescence signal of well A subtracted well B. The receptor occupancy rate (RO percent) of the same individual calculated with a zero-concentration sample. The Calculation Formula was $RO\%=[1-(MFI_B-MFI_A)/(MFI_{pre-dosing\ B}-MFI_{pre-dosing\ A})]\times100\%$.

Computational semi mechanistic pharmacology modeling

Model structure: A schematic of the *in vivo* model is shown in Fig. 7A. The model has three compartments: a central compartment, representing the circulation; a tumor compartment; and a peripheral compartment, representing other tissues into which the drug distributes. *Pharmacokinetics and transport*: Drug is dosed into the central compartment as an instantaneous bolus and distributes into and out of the tumor and peripheral compartments by first-order transport processes. Nonspecific elimination is modeled as a first-order process, with the same elimination rate is assumed for all compartments. *Drug binding*: The drug can bind to either 4-1BB or PD-L1 initially and can then crosslink to the other receptor. To model the 2 + 2 format of the ATG-101 antibody, ATG-101 simultaneously binds two 4-1BB receptors or PD-L1 receptors. The microscopic binding rate constants are doubled to account for the two binding sites on ATG-101. GEN1046 is a 1 + 1 format antibody and binds only one receptor at a time. Binding interactions are modeled via mass-action kinetics, with the exception of ATG-101 binding to PD-L1, which is modeled using a Hill equation inspired on-rate to better match the on-cell binding data presented in the Results section. *Receptors*: Each compartment contains a single $4\text{-}1BB^+$ cell population and a single PD-

$L1^+$ cell population. In the tumor, these cell populations are interpreted as tumor-infiltrating T-cells and tumor cells, respectively. In the central and peripheral compartments, these cell populations represent all cells expressing the receptor. Drug bound receptors internalize at the same rate as free receptors in all compartments.

Human Model parameterization: Typical pharmacokinetic parameters were used for both ATG-101 and GEN1046. The total amount and turnover of targets in the nominal patient was established by estimating the number of cells, the percent of receptor positive cells, the number of receptors per cell in each of the model compartments, and the internalization rate of the receptor. The E:T ratios in the tumor compartment were established by reviewing the density of $CD3^+$ T cells in a select panel of solid tumors in indications of interest. To determine the PD-L1 target burden, the model was benchmarked against clinical atezolizumab PK data. Atezolizumab PK was modeled by disabling 4-1BB binding and setting the PD-L1 binding affinity to literature-derived estimates and the half-life and transport parameters to typical parameters for IgG antibodies. A PD-L1 burden was chosen to strike a good balance between consistency with the PK data and prior literature-based estimates of the burden.

Statistical analysis

Statistical analyses were performed using GraphPad Prism Software, version 9.0. For in vitro cell binding and luciferase assay, nonlinear regression was performed and EC50 values were determined. A one-way analysis of variance (ANOVA) was performed for cytokines release study with more than two groups. A two-way ANOVA was performed to compare data with more than two groups treated with different conditions including cytokines release studies, tumor growth curves and lymphocyte change analyses. For mouse survival studies, the log-rank test (Mantel-Cox) were used. Differences with $P < 0.05$ were defined as statistically significant. Data are shown as means ± SEM (n = 2 or more).

Declarations

The protocol and any amendment(s) or procedures involving the care and use of animals in this study were reviewed and approved by the Institutional Animal Care and Use Committee (IACUC) prior to execution with an AUP number or IACUC approval number for each animal study. During the study, the care and use of animals were conducted in accordance with the regulations of the Association for Assessment and Accreditation of Laboratory Animal Care(AAALAC).All studies were conducted following an approved IACUC protocol.

Data and materials availability: All data are available in the main text or the supplementary materials.

Acknowledgments: We thank Innostar, Crown Bioscience, and Biocytogen for the support of several animal studies. We thank Tamara Etto and Nirmal Lorensuhewa for proof-reading the manuscript.

Author contributions: BHL and XWH designed the bispecific antibody construct. HJW and BHL conducted the first MC38 *in vivo* study and MC38 PD study. DF, MP and KS conducted the computational semi

mechanistic pharmacology modeling. HYW, TTL, YJR, PC conducted all the other experiments. HYW, TTL, YJR, MP, and BH analyzed data, made the figures and wrote the manuscript. KL, JM, XWH, BS and BH supervised the project team. BS and BH directed the study.

Competing interests: HYW, TTL, YJR, PC, KL, JM, BS and BH are employees and/or shareholders of Antengene Corporation Co., Ltd, Antengene (Hangzhou) Biologics Co., Ltd, Shanghai Antengene Corporation Limited, or Antengene Pty Ltd; Melbourne. DF, MP & KS are employees of Applied BioMath, LLC, Concord, MA. Applied BioMath provided modeling and simulation consulting services to Antengene Corporation, Shanghai. HJW, BHL and XWH are employees of Oricell Therapeutics Co., Ltd

Materials & Correspondence.

Materials request:

Bing Hou: bing.hou@antengene.com

*Corresponding author. Email: bing.hou@antengene.com; bo.shan@antengene.com; peterhe@oricell.com.

Author Informaton

Hui Yuwen and Huajing Wang: These authors contributed equally to this work

Affiliations:

Antengene Corporation Co., Ltd; Shaoxing, P.R.China.

Jay Mei, Bo Shan & Bing Hou

Shanghai Antengene Corporation Limited; Shanghai, P.R.China.

Hui Yuwen, Tengteng Li, Yijing, Ren &Peng Chen

Antengene (Hangzhou) Biologics Co., Ltd; Hangzhou, P.R.China.

Hui Yuwen, Tengteng Li, Yijing, Ren, Peng Chen, Bo Shan & Bing Hou

Antengene Pty Ltd; Melbourne, Australia.

Kevin Lynch

Oricell Therapeutics Co., Ltd; Shanghai, P.R.China.

Huajing Wang, Bohua Li, Xiaowen He

Applied BioMath LLC; Concord, MA, USA.

David Flowers, Marc Presler & Kalyanasundaram Subramanian

References

1. Chen DS, Mellman I. Elements of cancer immunity and the cancer-immune set point. *Nature* 2017, **541**(7637)**:** 321-330.

2. Pauken KE, Sammons MA, Odorizzi PM, Manne S, Godec J, Khan O*, et al.* Epigenetic stability of exhausted T cells limits durability of reinvigoration by PD-1 blockade. *Science* 2016, **354**(6316)**:** 1160-1165.

3. Sarmento-Ribeiro AB, Scorilas A, Goncalves AC, Efferth T, Trougakos IP. The emergence of drug resistance to targeted cancer therapies: Clinical evidence. *Drug resistance updates : reviews and commentaries in antimicrobial and anticancer chemotherapy* 2019, **47:** 100646.

4. Sen DR, Kaminski J, Barnitz RA, Kurachi M, Gerdemann U, Yates KB*, et al.* The epigenetic landscape of T cell exhaustion. *Science* 2016, **354**(6316)**:** 1165-1169.

5. Chester C, Sanmamed MF, Wang J, Melero I. Immunotherapy targeting 4-1BB: mechanistic rationale, clinical results, and future strategies. *Blood* 2018, **131**(1)**:** 49-57.

6. Kim HD, Park S, Jeong S, Lee YJ, Lee H, Kim CG*, et al.* 4-1BB Delineates Distinct Activation Status of Exhausted Tumor-Infiltrating CD8(+) T Cells in Hepatocellular Carcinoma. *Hepatology* 2020, **71**(3)**:** 955-971.

7. Leem G, Park J, Jeon M, Kim ES, Kim SW, Lee YJ*, et al.* 4-1BB co-stimulation further enhances anti-PD-1-mediated reinvigoration of exhausted CD39(+) CD8 T cells from primary and metastatic sites of epithelial ovarian cancers. *Journal for immunotherapy of cancer* 2020, **8**(2)**:** e001650.

8. Woroniecka KI, Rhodin KE, Dechant C, Cui X, Chongsathidkiet P, Wilkinson D*, et al.* 4-1BB Agonism Averts TIL Exhaustion and Licenses PD-1 Blockade in Glioblastoma and Other Intracranial Cancers. *Clinical cancer research : an official journal of the American Association for Cancer Research* 2020, **26**(6)**:** 1349-1358.

9. Ho SK, Xu Z, Thakur A, Fox M, Tan SS, DiGiammarino E*, et al.* Epitope and Fc-Mediated Cross-linking, but Not High Affinity, Are Critical for Antitumor Activity of CD137 Agonist Antibody with Reduced Liver Toxicity. *Molecular cancer therapeutics* 2020, **19**(4)**:** 1040-1051.

10. Segal NH, Logan TF, Hodi FS, McDermott D, Melero I, Hamid O*, et al.* Results from an Integrated Safety Analysis of Urelumab, an Agonist Anti-CD137 Monoclonal Antibody. *Clinical cancer research : an official journal of the American Association for Cancer Research* 2017, **23**(8)**:** 1929-1936.

11. Geuijen C, Tacken P, Wang LC, Klooster R, van Loo PF, Zhou J*, et al.* A human CD137xPD-L1 bispecific antibody promotes anti-tumor immunity via context-dependent T cell costimulation and checkpoint blockade. *Nature communications* 2021, **12**(1)**:** 4445.

12. Li Y, Tan S, Zhang C, Chai Y, He M, Zhang CW*, et al.* Limited Cross-Linking of 4-1BB by 4-1BB Ligand and the Agonist Monoclonal Antibody Utomilumab. *Cell reports* 2018, **25**(4)**:** 909-920 e904.

13. Segal NH, Gopal AK, Bhatia S, Kohrt HE, Levy R, Pishvaian MJ*, et al.* A phase 1 study of PF-05082566 (anti-4-1BB) in patients with advanced cancer. *Journal of Clinical Oncology* 2014, **32**(15_suppl)**:** 3007-3007.

14. Tolcher AW, Sznol M, Hu-Lieskovan S, Papadopoulos KP, Patnaik A, Rasco DW*, et al.* Phase Ib Study of Utomilumab (PF-05082566), a 4-1BB/CD137 Agonist, in Combination with Pembrolizumab (MK-3475) in Patients with Advanced Solid Tumors. *Clinical cancer research : an official journal of the American Association for Cancer Research* 2017, **23**(18)**:** 5349-5357.

15. Hinner MJ, Aiba RSB, Jaquin TJ, Berger S, Durr MC, Schlosser C*, et al.* Tumor-Localized Costimulatory T-Cell Engagement by the 4-1BB/HER2 Bispecific Antibody-Anticalin Fusion PRS-343. *Clinical cancer research : an official journal of the American Association for Cancer Research* 2019, **25**(19)**:** 5878-5889.

16. Rajendran S, Li Y, Ngoh E, Wong HY, Cheng MS, Wang CI*, et al.* Development of a Bispecific Antibody Targeting CD30 and CD137 on Hodgkin and Reed-Sternberg Cells. *Frontiers in oncology* 2019, **9:** 945.

17. You G, Lee Y, Kang YW, Park HW, Park K, Kim H*, et al.* B7-H3x4-1BB bispecific antibody augments antitumor immunity by enhancing terminally differentiated CD8(+) tumor-infiltrating lymphocytes. *Science advances* 2021, **7**(3).

18. Dahlman A, Nelson M, Bannink J, Johnson S, Werchau D, Nilsson A*, et al.* Abstract 2380: Preclinical safety and efficacy of a tumor-directed T cell activating 4-1BB x 5T4 ADAPTIR™ bispecific antibody. *Cancer Research* 2019, **79**(13_Supplement)**:** 2380-2380.

19. Liu L, Huang L, Long V, Yang Y, Burns R, Li J*, et al.* Abstract 554: Tumor-antigen 5T4-dependent activation of the CD137 costimulatory pathway by bispecific 5T4 x CD137 x CD137 TRIDENT™ molecules. *Cancer Research* 2019, **79**(13_Supplement)**:** 554-554.

20. Darvin P, Toor SM, Sasidharan Nair V, Elkord E. Immune checkpoint inhibitors: recent progress and potential biomarkers. *Experimental & molecular medicine* 2018, **50**(12)**:** 1-11.

21. Wang J, Sun J, Liu LN, Flies DB, Nie X, Toki M*, et al.* Siglec-15 as an immune suppressor and potential target for normalization cancer immunotherapy. *Nature medicine* 2019, **25**(4)**:** 656-666.

22. Vezys V, Penaloza-MacMaster P, Barber DL, Ha SJ, Konieczny B, Freeman GJ*, et al.* 4-1BB signaling synergizes with programmed death ligand 1 blockade to augment CD8 T cell responses during chronic viral infection. *Journal of immunology* 2011, **187**(4)**:** 1634-1642.

23. Alsaab HO, Sau S, Alzhrani R, Tatiparti K, Bhise K, Kashaw SK*, et al.* PD-1 and PD-L1 Checkpoint Signaling Inhibition for Cancer Immunotherapy: Mechanism, Combinations, and Clinical Outcome. *Frontiers in pharmacology* 2017, **8:** 561.

24. Liu R, Oldham RJ, Teal E, Beers SA, Cragg MS. Fc-Engineering for Modulated Effector Functions-Improving Antibodies for Cancer Treatment. *Antibodies* 2020, **9**(4).

25. Hashimoto K. CD137 as an Attractive T Cell Co-Stimulatory Target in the TNFRSF for Immuno-Oncology Drug Development. *Cancers* 2021, **13**(10)**:** 2288.

26. Shimabukuro-Vornhagen A, Godel P, Subklewe M, Stemmler HJ, Schlosser HA, Schlaak M*, et al.* Cytokine release syndrome. *Journal for immunotherapy of cancer* 2018, **6**(1)**:** 56.

27. Bohua Li HW, Xiaowen He. ANTI-PD-L1 ANTIBODY AND USE THEREOF *WO 2019/196309 A1* 2019.

28. Betts A, van der Graaf PH. Mechanistic Quantitative Pharmacology Strategies for the Early Clinical Development of Bispecific Antibodies in Oncology. *Clinical pharmacology and therapeutics* 2020, **108**(3)**:** 528-541.

29. Dahlman A, Michelle Nelson, Jeannette Bannink, Starrla Johnson, Doreen Werchau, Anneli Nilsson*, et al.* Abstract 2380: Preclinical safety and efficacy of a tumor-directed T cell activating 4-1BB x 5T4 ADAPTIR™ bispecific antibody. *Cancer Res* 2019, **79**(13_Supplement)**:** 2380.

30. Fraisse J, Dinart D, Tosi D, Bellera C, Mollevi C. Optimal biological dose: a systematic review in cancer phase I clinical trials. *BMC cancer* 2021, **21**(1)**:** 60.

31. Aix SP, Calvo E, Moreno V, Garralda E, Cervantes A, Ramalingam S*, et al.* 516 Peripheral and tumoral immune activity in the expansion part of the first-in-human DuoBody®-PD-L1×4–1BB (GEN1046) trial. *Journal for immunotherapy of cancer* 2021, **9**(Suppl 2)**:** A546-A546.

32. Muik A, Garralda E, Altintas I, Gieseke F, Geva R, Ben-Ami E*, et al.* Preclinical Characterization and Phase I Trial Results of a Bispecific Antibody Targeting PD-L1 and 4-1BB (GEN1046) in Patients with Advanced Refractory Solid Tumors. *Cancer discovery* 2022, **12**(5)**:** 1248-1265.

33. Bajaj G, Nazari F, Presler M, Thalhauser C, Forssmann U, Jure-Kunkel M*, et al.* 786 Dose selection for DuoBody®-PD-L1×4-1BB (GEN1046) using a semimechanistic pharmacokinetics/pharmacodynamics model that leverages preclinical and clinical data. *Journal for immunotherapy of cancer* 2021, **9**(Suppl 2)**:** A821-A821.

34. Genmab. Safety and Efficacy Study of GEN1046 as a Single Agent or in Combination With Another Anti-cancer Therapy for Treatment of Recurrent (Non-small Cell) Lung Cancer. *NCT05117242* 2021.

35. Inhibrx I. financial results for the fourth quarter and fiscal year. 2020.

36. Inhibrx I. Study of INBRX-105 in Patients With Solid Tumors (PDL1x41BB). *NCT03809624* 2019.

37. Lei Q, Wang D, Sun K, Wang L, Zhang Y. Resistance Mechanisms of Anti-PD1/PDL1 Therapy in Solid Tumors. *Frontiers in cell and developmental biology* 2020, **8:** 672.

38. Sade-Feldman M, Jiao YJ, Chen JH, Rooney MS, Barzily-Rokni M, Eliane JP*, et al.* Resistance to checkpoint blockade therapy through inactivation of antigen presentation. *Nature communications* 2017, **8**(1)**:** 1136.

39. Shin DS, Zaretsky JM, Escuin-Ordinas H, Garcia-Diaz A, Hu-Lieskovan S, Kalbasi A*, et al.* Primary Resistance to PD-1 Blockade Mediated by JAK1/2 Mutations. *Cancer discovery* 2017, **7**(2)**:** 188-201.

40. Skoulidis F, Goldberg ME, Greenawalt DM, Hellmann MD, Awad MM, Gainor JF*, et al.* STK11/LKB1 Mutations and PD-1 Inhibitor Resistance in KRAS-Mutant Lung Adenocarcinoma. *Cancer discovery* 2018, **8**(7)**:** 822-835.

41. Petroni G, Buque A, Coussens LM, Galluzzi L. Targeting oncogene and non-oncogene addiction to inflame the tumour microenvironment. *Nature reviews Drug discovery* 2022.

42. Bejarano L, Jordao MJC, Joyce JA. Therapeutic Targeting of the Tumor Microenvironment. *Cancer discovery* 2021, **11**(4)**:** 933-959.

43. Yu JW, Bhattacharya S, Yanamandra N, Kilian D, Shi H, Yadavilli S*, et al.* Tumor-immune profiling of murine syngeneic tumor models as a framework to guide mechanistic studies and predict therapy response in distinct tumor microenvironments. *PloS one* 2018, **13**(11)**:** e0206223.

44. Chen P, Liu Y, Deng M, Wang J, Hoenemann D, Lynch K*, et al.* 608 Synergistic effect of the combination of ATG-017, an ERK1/2 inhibitor, and immune checkpoint inhibitor in preclinical cancer models. *Journal for immunotherapy of cancer* 2021, **9**(Suppl 2)**:** A638-A638.

45. Koyama S, Akbay EA, Li YY, Herter-Sprie GS, Buczkowski KA, Richards WG*, et al.* Adaptive resistance to therapeutic PD-1 blockade is associated with upregulation of alternative immune checkpoints. *Nature communications* 2016, **7:** 10501.

46. Oweida A, Hararah MK, Phan A, Binder D, Bhatia S, Lennon S*, et al.* Resistance to Radiotherapy and PD-L1 Blockade Is Mediated by TIM-3 Upregulation and Regulatory T-Cell Infiltration. *Clinical cancer research : an official journal of the American Association for Cancer Research* 2018, **24**(21)**:** 5368-5380.

47. Johnson DB, Estrada MV, Salgado R, Sanchez V, Doxie DB, Opalenik SR*, et al.* Melanoma-specific MHC-II expression represents a tumour-autonomous phenotype and predicts response to anti-PD-1/PD-L1 therapy. *Nature communications* 2016, **7:** 10582.

48. Johnson DB, Nixon MJ, Wang Y, Wang DY, Castellanos E, Estrada MV, *et al.* Tumor-specific MHC-II expression drives a unique pattern of resistance to immunotherapy via LAG-3/FCRL6 engagement. *JCI insight* 2018, **3**(24)**:** e120360.

49. Antengene. A Study of Evaluating the Safety and Efficacy of ATG-101 in Patients With Metastatic/Advanced Solid Tumors and Mature B-cell Non-Hodgkin Lymphomas (PROBE). *NCT04986865* 2021.

Figures

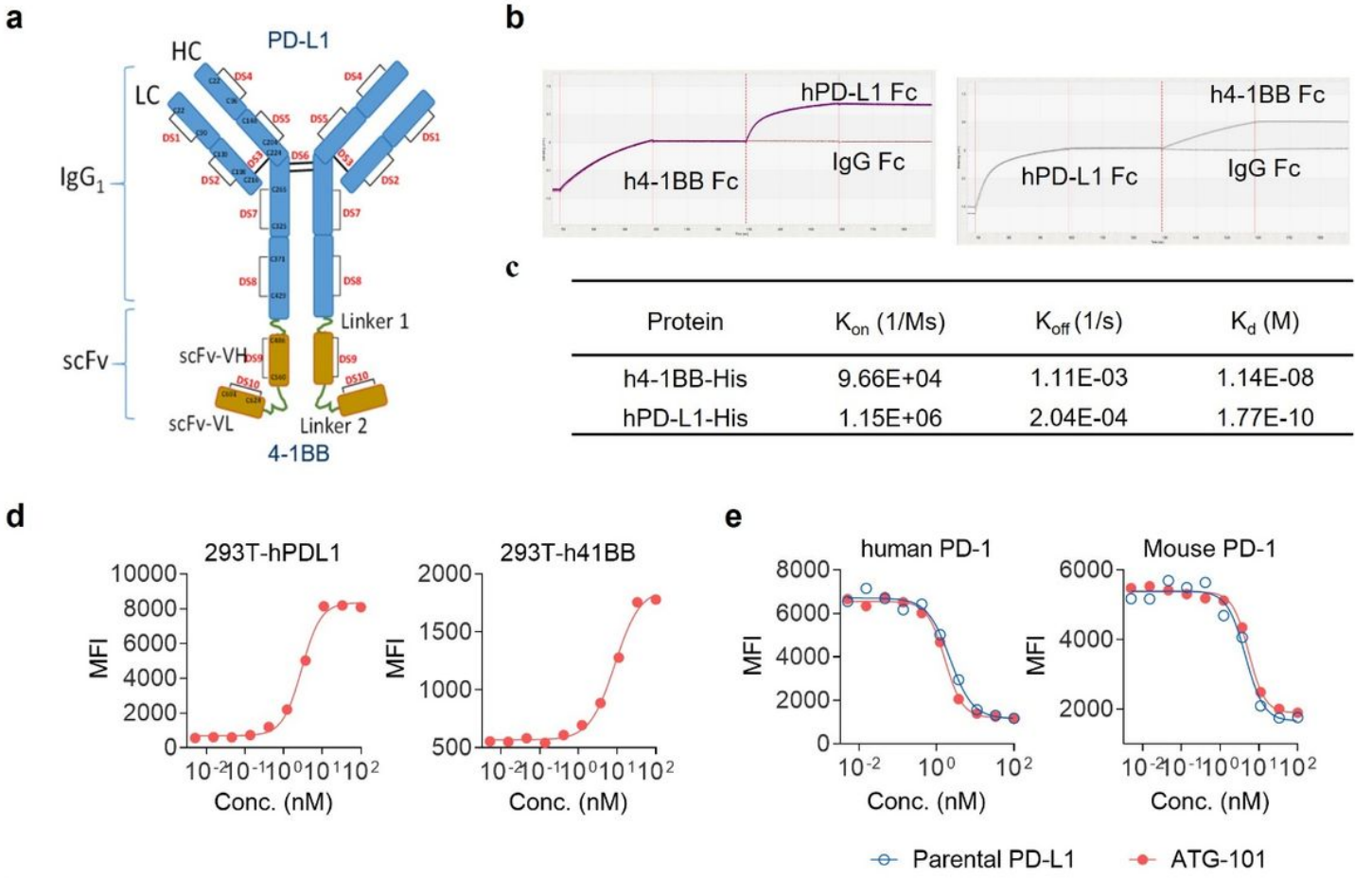

c

Protein	K_{on} (1/Ms)	K_{off} (1/s)	K_d (M)
h4-1BB-His	9.66E+04	1.11E-03	1.14E-08
hPD-L1-His	1.15E+06	2.04E-04	1.77E-10

f

	hFcRⅠ	hFcRⅡA	hFcRⅡB	hFcRⅢA	hFcRn (PH=6.0)
Affinity(Kd)	N.D	N.D	N.D	N.D	1.83E-08

Figure 1

ATG-101 binds to hPD-L1 and h4-1BB simultaneously.

(**a**) Structure of ATG-101 bispecific antibody. ATG-101 employs the IgG(H)-scFv structure, with the Fab arm targeting PD-L1 and the scFv targeting 4-1BB linked to the C-terminus of the F_C domain. The amino

acid of linker 1 and linker 2 is $(G_4S)_3$ and $AST(G_4S)_3$, respectively. DS, disulphide bond (**b**) Binding capability of ATG-101 to hPD-L1/h4-1BB as determined by ForteBio. ATG-101 was immobilized on the biosensor, and the h4-1BB Fc (left panel) or hPD-L1 Fc (right panel) protein was injected first to bind ATG-101, whereafter hPD-L1 Fc (left panel) or h4-1BB Fc (right panel) protein was injected to bind. IgG-Fc was used as negative control. (**c**) Kinetics parameter of binding affinity of ATG-101 to hPD-L1/h4-1BB. K_{on}, association rate constant; K_{off}, dissociation rate constant; K_d, dissociation constant, $K_d = K_{off}/K_{on}$. (**d**) Binding of ATG-101 to 293T-hPDL1 (left) or 293T-h41BB (right). (**e**) Blockade of the binding of biotinylated PD-1 protein to PD-L1 over expressed CHO cells by ATG-101 or parental PDL1 Ab. Blocking IC_{50} of parental antibody and ATG-101 for human and mouse was 1.65 nM and 2.21nM, 5.44 nM and 4.52 nM respectively. (**f**) Summary of binding affinity of ATG-101 to Fcγ

receptor and FcRn as determined by ForteBio. ND, not detected.

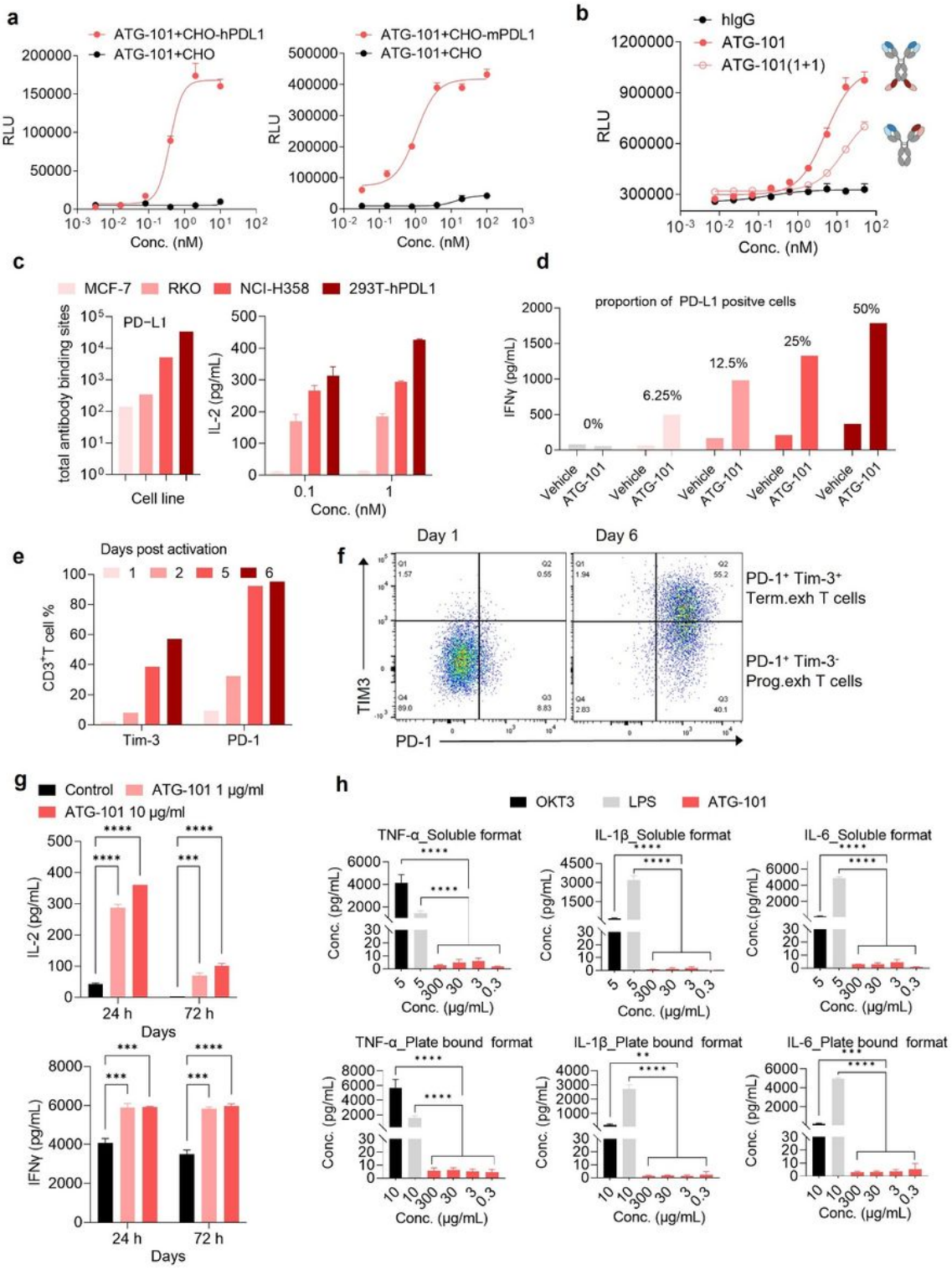

Figure 2

ATG-101 activates 4-1BB signaling upon PD-L1 crosslinking.

(**a, b**) The 4-1BB agonistic activity of ATG-101 in NF-κB luciferase assay. (**a**) 293T-h41BB-NF-κB-Luc cells were incubated with ATG-101 and CHO-hPDL1 (left) or CHO-mPDL1 (right) for 24 hours. Wild type CHO cells as negative control (*n* = 3). (**b**) 4-1BB activation by ATG-101, bivalent PD-L1×4-1BB bsAb [ATG-

101(1+1)] or isotype control antibodies in 293T-h41BB-NF-κB-Luc cells with the presence of 293T-hPDL1 (n = 2). Tetravalent and bivalent ATG-101 activated 4-1BB signal pathway with EC_{50} of 5.25 nM and 15.44 nM, respectively. (**c**) Effect of ATG-101 on IL-2 release by $CD8^+$ T cells with the presence of PD-L1 positive cell lines. PD-L1 densities (total antibody binding sites) on MCF-7, RKO, NCI-H358 and 293T-hPDL1 cell surfaces were determined using QIFIKIT (left). All the indicated cells co-cultured with $CD8^+$ T cells and ATG-101 for 3 days, and supernatants were harvested for IL-2 ELISA to assess T cell activation (n = 2, right). (**d**) ATG-101-induced IFNγ release by human primary $CD8^+$ T cells co-culturing with varying proportions of PD-L1 positive cells. HEK293-PDL1 cells were mixed with parental HEK293 at different proportions. The IFNγ release was detected by ELISA. (**e, f**) The expression dynamics of PD-1 and Tim-3 on $CD3^+$ T cell surface after activation by anti-CD3/CD28, detected by flow cytometry. The percentage of PD-1 or Tim-3 positive T cells (E), and (F) representative flow cytometry dot-plots of T cell subsets on day 1 and day 6 after activation. Terminally exhausted T cells ($PD\text{-}1^+Tim\text{-}3^+$, Term.exh T cells) and progenitor exhausted T cells ($PD\text{-}1^+Tim\text{-}3^-$, Prog.exh T cells) were labeled. (**g**) ATG-101 stimulates IL-2 and IFNγ production by exhausted T cells. 6 days after activation, exhausted T cells were treated with ATG-101 or isotype control for 1 or 3 days, and IL-2 and IFNγ release were detected by ELISA (n = 2). (**h**) Cytokine release by PMBCs from healthy donors (n = 6) treated with anti-CD3 (OKT3), LPS or ATG-101 in both soluble and plate-bound formats. Cytokines were analyzed after treatment with 48 hours using electrochemiluminescence immunoassay. Data are presented as means ± SEM. Statistical analysis used two-way ANOVA, *P < 0.05, ** P < 0.01, *** P < 0.001, ****P < 0.0001.

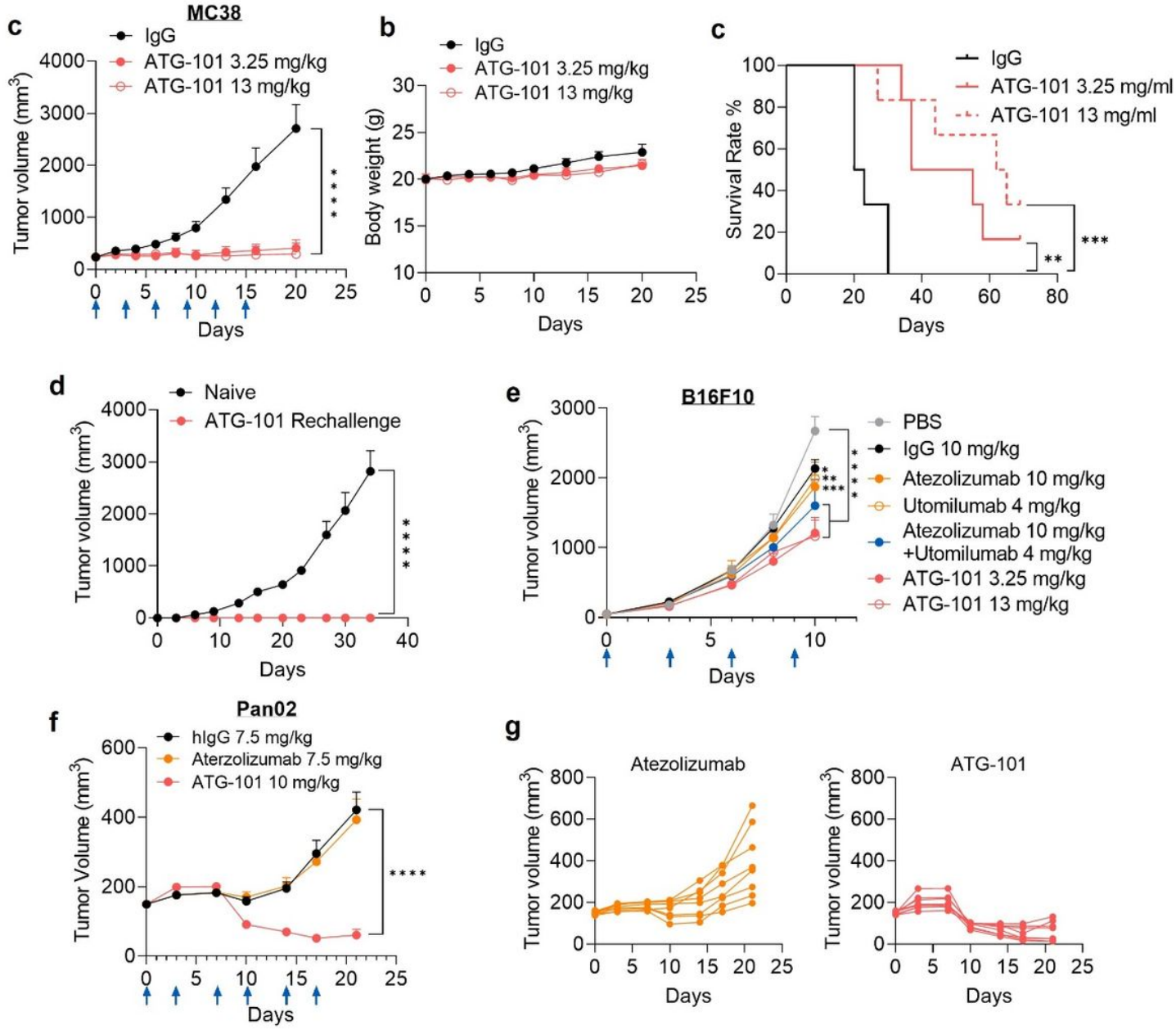

Figure 3

ATG-101 shows anti-tumor efficacy in vivo.

(**a-d**) MC38 colon cancer xenograft model on h4-1BB humanized mice (C57BL/6). When the tumors volume reached about 239 mm^3 (**a-c**), the mice were grouped and treated with indicated antibody twice a week for 2 weeks (*n* = 5 for PBS, *n* = 6 for the other groups). Growth curves of MC38 tumor (**A**), body weight change (**b**) and Kaplan–Meier survival plot of mice (**c**). (**d**) Tumor free mice from (A) were rechallenged with MC38. ATG-101-cured (*n* = 2) or naive mice (*n* = 3) were injected subcutaneously with 5×10^5 MC38 cells in the opposite flank on day 42. Tumors were measured twice a week (**e**) B16F10

melanoma model or (**f**) Pan02 pancreatic tumor model on h4-1BB humanized mice. The mice were intraperitoneally injected with tested articles once every three days (n = 8). In (a), (b), (d), (e) and (f), means ± SEM are shown. Statistical

analysis used two-way-ANOVA for tumor growth comparison and log-rank test (Mantel-Cox) for survival analysis, *P < 0.05, ** P < 0.01, *** P < 0.001, ****P < 0.0001. In the tumor growth curves, only P values on the last day were shown except for B16F10 whose P value on day 10 was shown.

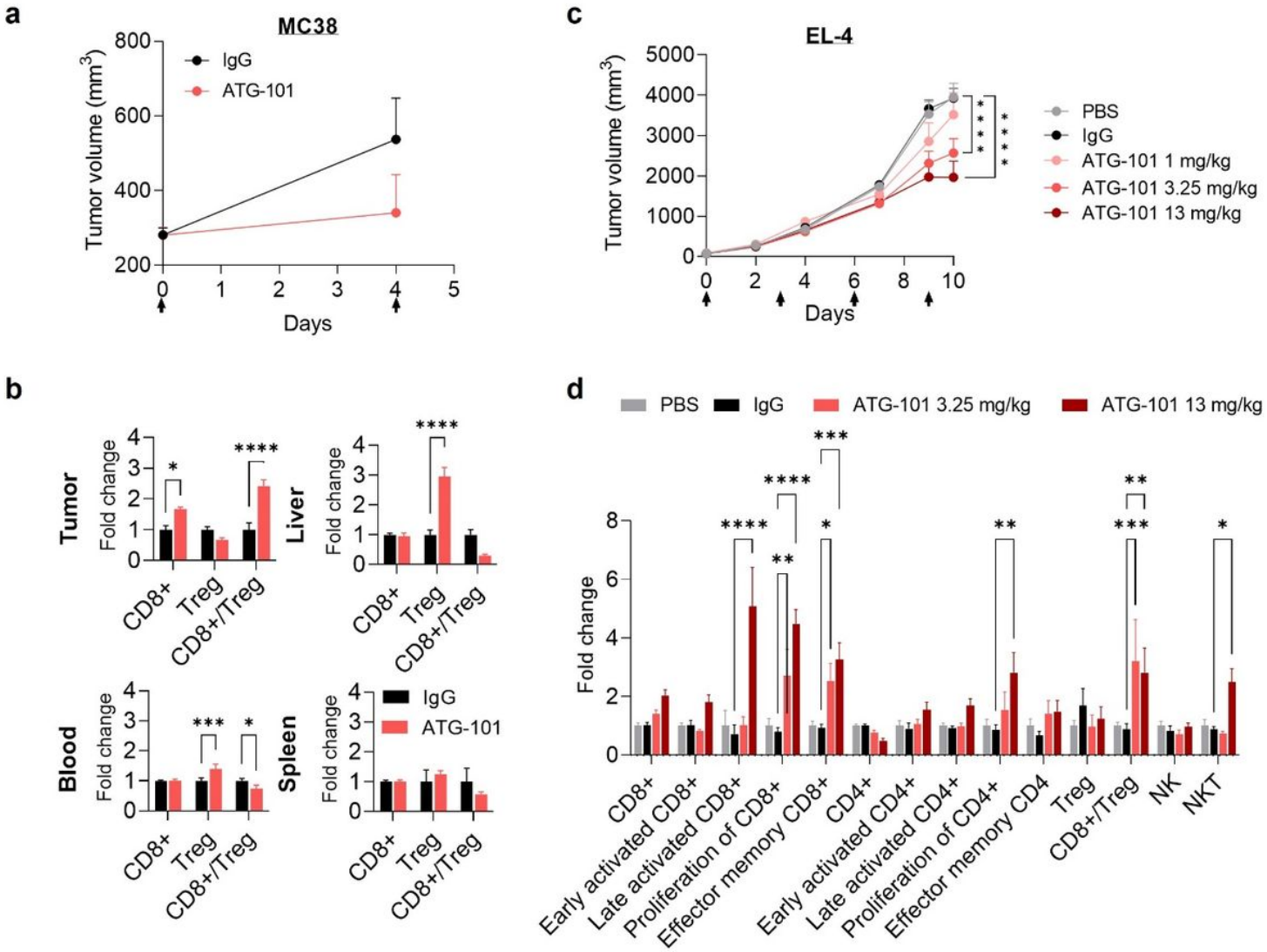

Figure 4

ATG-101 enhances the anti-tumor immunity in the tumor microenvironment.

(**a**)Growth curves of MC38 colon tumors on h4-1BB humanized mice (C57BL/6). When the tumor volume reached about 281 mm3, the mice (n = 4) were intraperitoneally injected with IgG or ATG-101 on day 0 and day 4, as indicated by arrow (**b**) Normalized CD8+ T cell and Treg cell number in tumor, liver, blood, and spleen from (a). 48 hours after the last administration, the samples were collected. Fold change indicates ATG-101 treatment group vs. mean value of IgG control group. (**c**) Growth curves of EL4 T cell

lymphoma on h4-1BB humanized mice (C57BL/6). When the tumors size reached about 71 mm3, the mice (n = 8) were grouped and treated with PBS, IgG or ATG-101. (**d**) Normalized tumor infiltrating lymphocyte analysis result from tumors from (c). Fold change indicates IgG or ATG-101 treatment group vs. mean valve of PBS group. Means ± SEM are shown. Asterisks indicated P values as *P < 0.05, ** P < 0.01, *** P < 0.001, ****P < 0.0001 by two-way ANOVA. In the tumor growth curves, only P values on the last day were shown.

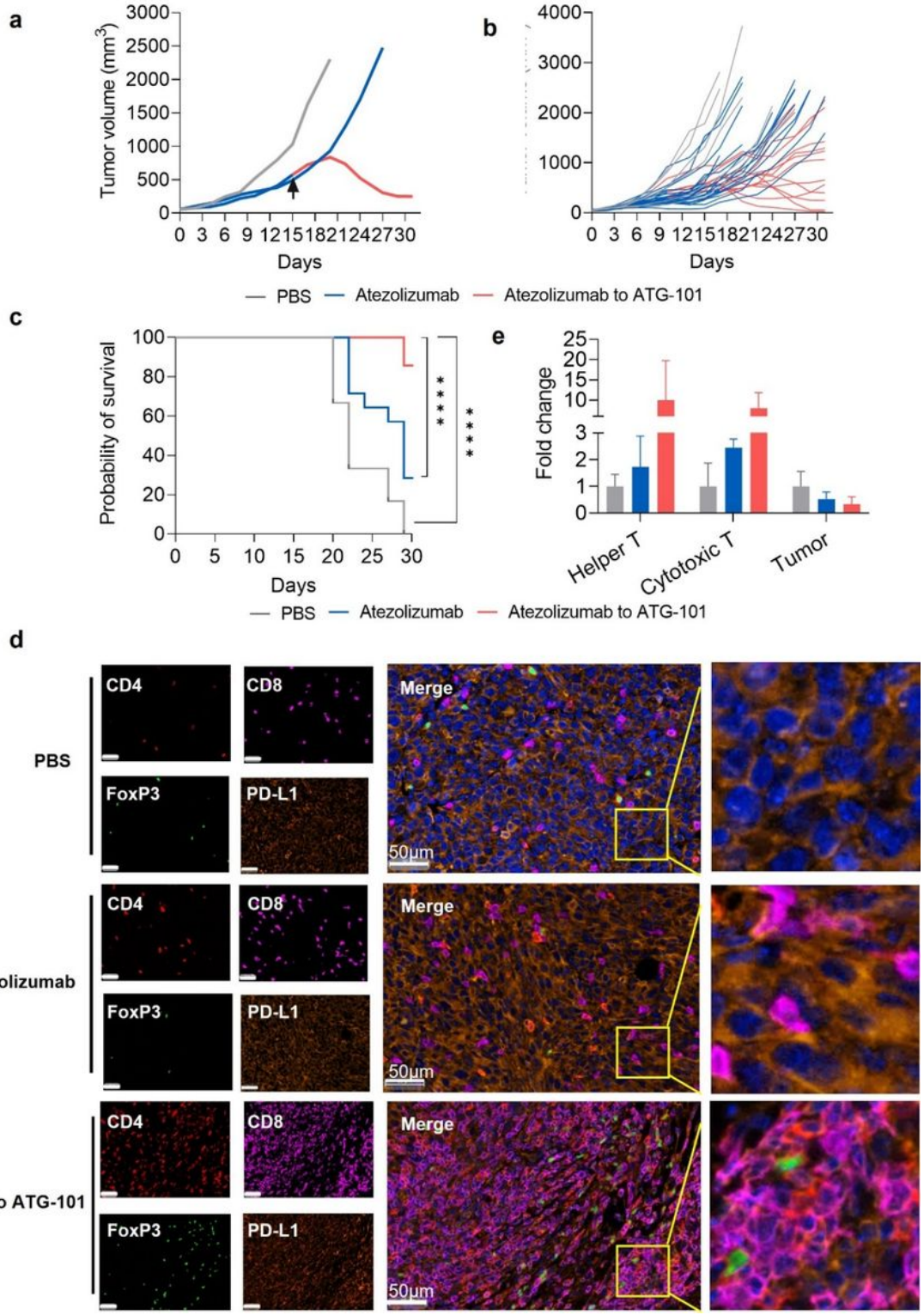

Figure 5

ATG-101 demonstrates in vivo efficacy in MC38 tumor model progressing on anti-PD-L1 treatment, enhancing the anti-tumor immunity in the tumor microenvironment.

(**a**)Representative individual MC38 tumor growth curve. The mice weretreated with PBS (black), 10 mg/kg atezolizumab only (red) or mice initially treated with 10 mg/kg atezolizumab and switched to 13 mg/kg ATG-101 upon disease progression (red to green); the arrow indicates the day switching atezolizumab to ATG-101. (**b**) Individual tumor growth spaghetti plots of mice treated with PBS (black, *n* = 6), atezolizumab only (red, *n* = 14), and atezolizumab to ATG-101 (red-green, *n* = 14). (**c**) Survival data of mouse shown in (b), ****$P < 0.0001$ by log-rank (Mantel-Cox) test. (**d**) Representative images of multiplex immunohistochemistry (IHC) staining of tumor samples collected from mouse from (b). The tumor slices were stained for CD4 (helper T cell, red), CD8 (effector T cell, purple), Foxp3 (Treg, green), and PD-L1 (cancer cells, dark orange). Nucleus were labelled with DAPI (blue). Areas highlighted in the merged images are enlarged. Scale bars are 50 μm. (**e**) Quantitative analysis of cell populations shown in (e). Fold change indicates atezolizumab only group or atezolizumab to ATG-101 group vs. mean valve of PBS group. Means ± SEM are shown. *n* = 3 in PBS and atezolizumab group; *n* = 6 in ATG-101 group.

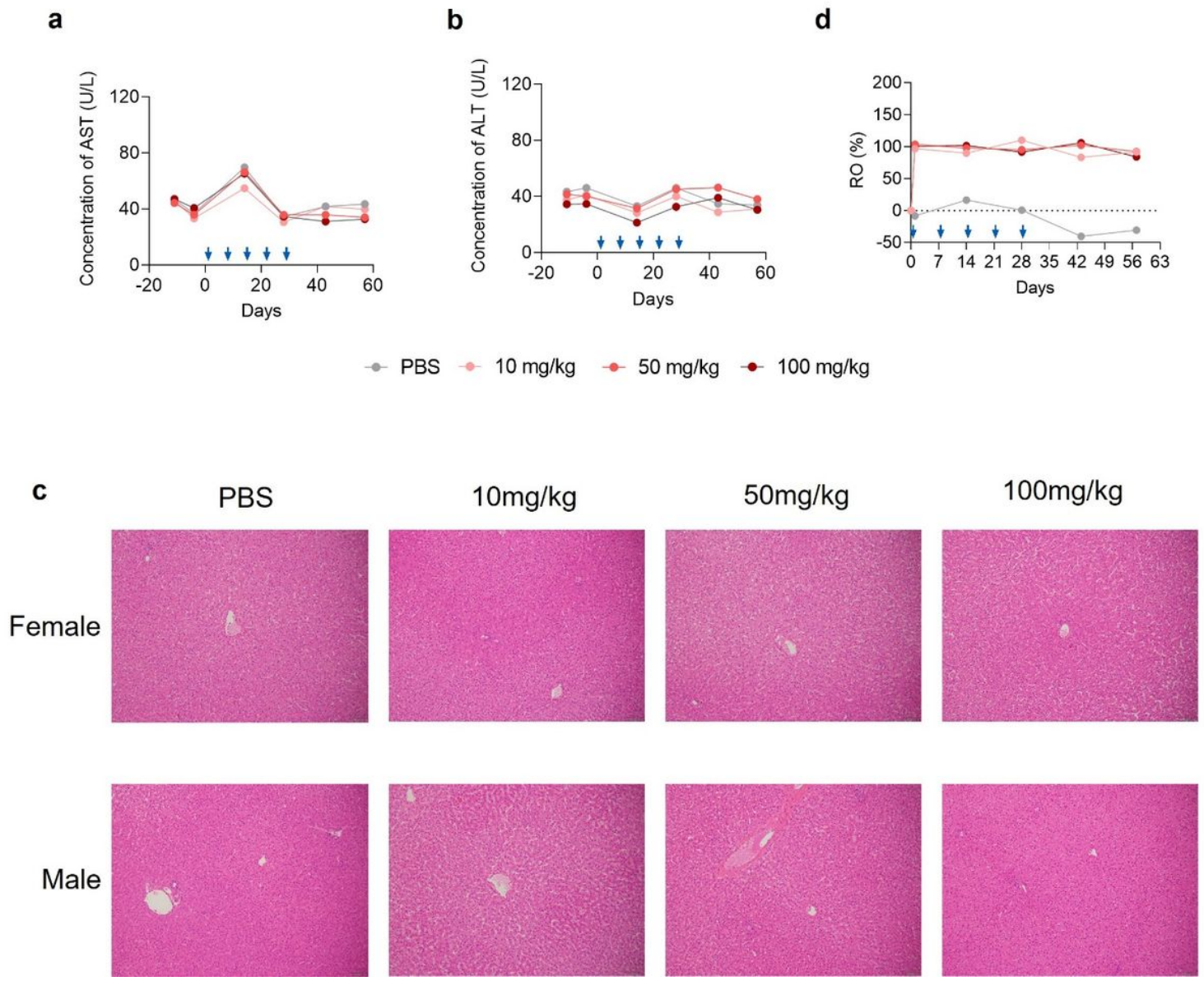

Figure 6

Safety of ATG-101 in a repeat dose non-human primate study.

(**a, b**) Mean serum concentrations of AST (**a**) and ALT (**b**) of cynomolgus monkeys over the Study period at the indicated doses. ATG-101 was given to cynomolgus monkeys (*n* = 10 per group, 5 males and 5 females) once a week as indicated by the arrows, followed by a 4-week recovery period. Blood samples were collected before feeding. (**c**) PD-L1 receptor occupancy on $CD3^{+}$T cells over the study period at the indicated doses. AF647 labeled parental anti-PD-L1 antibody was employed to assist in the measurement of the ratio of free receptor. (*n* = 10 per group, 5 female mice and 5 male mice.) (**d**) Representative images of hematoxylin-eosin (HE) staining of liver tissue collected from the animals in the study.

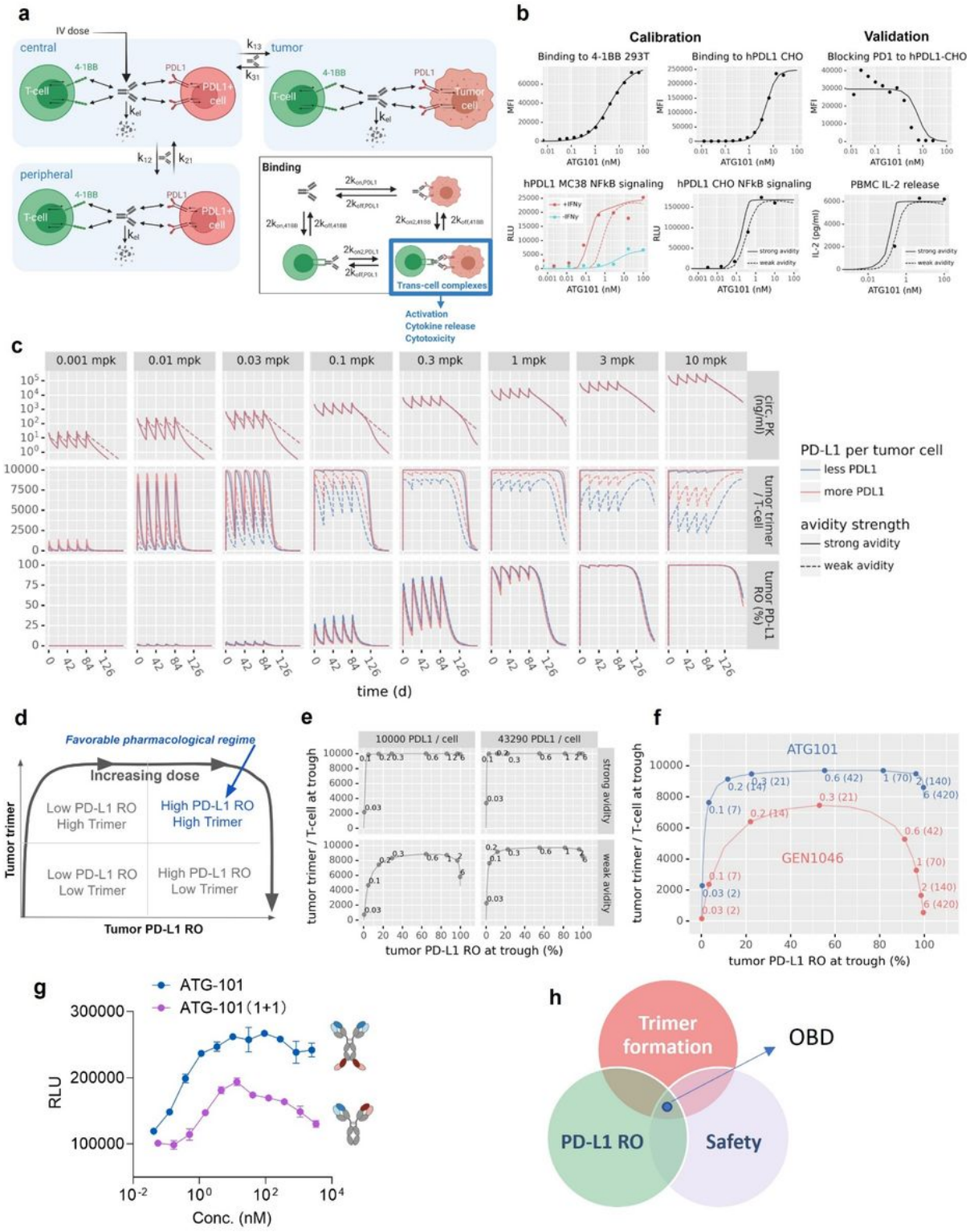

Figure 7

Semi-mechanistic pharmacology model of ATG-101.

(a) In vitro model diagram. The model has three compartments: a central compartment,

representing the circulation; a tumor compartment; and a peripheral compartment, representing other tissues into which the drug distributes. Drug bind to either receptor initially, then cross-link to the other. Trans-cell complexes (i.e., trimers) are assumed to drive the pharmacological activity of ATG-101. (**b**) In vitro model calibration and validation. In vitro cell binding was used to calibrate the monovalent binding affinities, and NF-κB signaling assays were used to calibrate the crosslinking rate of ATG-101. Serial dilutions of ATG-101 were incubated with 293T-h41BB-NF-κB-Luc or CHO-hPDL1. NF-κB signaling assays was detected in the presence or absence IFNγ stimulation on hPD-L1 expressing MC38 cells. Two crosslinking rates (“strong avidity” and “weak avidity” lines) were calibrated to capture the uncertainty in the parameter (calibration, left panel). The model was validated with PD-1/PD-L1 blocking assays (validation, right panel). Lines show model predictions and points show data values for CHO cells expressing hPD-L1 and mPD-L1. (**c**) In vivo human solid tumor model predictions The in vivo human solid tumor patient model was used to simulate five doses administered every three weeks at levels from 0.001 to 10 mg/kg and predict circulating free drug levels, tumor trimer formation, and tumor PD-L1 receptor occupancy over time. The crosslinking rate and PD-L1 per tumor cell were varied to include the effects of parameter uncertainty and variability in the predictions. (**d-f**) Human model simulated trimer versus PD-L1 RO. (d) Schematic representing the pharmacological regimes between trimer formation and receptor occupancy of PD-L1. (e) Simulations of trimer formation vs PD-L1 RO in high vs low PD-L1 density and high vs low crosslinking avidity for ATG-101 at Q3W (f) As in the previous panel, the x axis indicates the tumor cell PD-L1 RO at trough. The y axis indicates the number of trimers per tumor-infiltrating T-cell at trough. Color indicates molecule and crosslinking strength. Points indicate select doses, with text indicating the dose level in mg/kg outside the parentheses and mg inside the parentheses. Panels indicate the dosing frequency. A body weight of 70 kg was assumed. Avidity values are chosen to be conservative for the comparison (i.e., the favorable avidity for GEN1046 and the less favorable avidity for ATG-101). (**g**) NF-κB signaling assays of tetravalent ATG-101 and bivalent ATG-101 in 4-1BB activation. Serial dilutions of tetravalent ATG-101 (red) or bivalent ATG-101 (1+1) (blue) were incubated with 293T-h41BB-NF-κB-Luc and 293T-hPDL1 cells for 24 hours. The luciferase activity was analyzed by measuring luminescence. RLU, relative light unit. (**h**) Schematic outlining the features of the optimal dose of ATG-101. There is a “sweet spot” between trimer formulation, PD-L1 RO, and bispecific antibody safety. ATG-101's tetravalent structure, as well as its affinity for PD-L1 and 4-1BB, ensures a high degree of trimer formation and PD-L1 RO at the same dose level, while also ensuring safety.

Supplementary Files

This is a list of supplementary files associated with this preprint. Click to download.

- SupplementaryMaterialNC2022.docx